A numerical strategy for investigating the kinetic response of stimulus-responsive hydrogels

John Dolbow,[†] Eliot Fried,[‡] Huidi Ji[†]

[†]Department of Civil and Environmental Engineering
Duke University
Durham, NC 27708-0287, USA

[‡]Department of Mechanical and Aerospace Engineering
Washington University in St. Louis
St. Louis, MO 63130-4899, USA

June 14, 2004

Abstract

We present a strategy for obtaining numerical solutions to a system of nonlinear, coupled evolution equations describing volume transitions in stimulus-responsive hydrogels (SRHs). The theory underlying our sharp-interface model of phase transitions in SRHs is provided along with the assumptions leading to the specialized formulation that is the starting point for the numerical method. The discrete formulation is then developed with a hybrid eXtended Finite-Element/Level-Set Method (XFE/LSM). Domain-integral methodologies are used consistently to extract interfacial quantities such as the mechanical driving traction, the jump in the normal component of the solute flux, and requisite geometric information. Several benchmark studies are provided to demonstrate the accuracy and robustness of the numerical strategy. We then investigate various features of SRH kinetics including the regimes of unstable and stable phase transitions, surface pattern formation, and bulk phase separation.

Keywords: Extended finite element; Level set; Hydrogels; Configurational forces; Sharp interface

1 Introduction

A hydrogel is a cross-linked, macromolecular polymer network immersed in a solvent. *Stimulus-responsive hydrogels* (SRHs) are synthesized to exhibit large, reversible volume changes in response to relatively small changes in environmental stimuli. Much of the current interest in these materials is motivated by microscale applications because diffusion path-lengths at those scales enable actuation times on the order of milliseconds. Recent examples of such applications include microgel drug carriers/pumps for therapeutic biomedical applications (Eichenbaum et al., 1999), autonomous microfluidic actuators (Beebe et al., 2000), and optical switches (Pardo-Yissar et al., 2001). While applications and experimental studies of miniaturized SRH-based systems continue to emerge, predictive models and associated numerical strategies have lagged.

Many models for SRH swelling are based on a collective diffusion assumption originally proposed by Tanaka and Fillmore (1979). Though capable of providing predictions that are consistent with experiments, collective diffusion does not explicitly account for experimentally observed phase interfaces separating swelled and collapsed phases. More

recent efforts by Tomari and Doi (1995) (see also Tomari and Doi (1994)) have employed sharp-interface assumptions and Flory–Huggins type free-energy functionals to describe SRH kinetics. In previous work (Dolbow et al., 2004), we presented a continuum-based sharp-interface model for chemically-induced phase transitions in SRHs. Using an eXtended Finite-Element/Level-Set Method (XFE/LSM), we studied the transition kinetics of spherical gel specimens. The key results of our analysis include breakthrough curves delineating ranges of stable, two-phase states, and the numerical confirmation of experimentally observed swelling times proportional to the square of the specimen radius.

The eXtended Finite-Element Method (X-FEM) augments a classical set of piecewise-polynomial shape functions with local, generally non-polynomial functions possessing desirable approximation properties in the vicinity of a feature of interest. This concept was first introduced by Duarte and Oden (1995) in the context of an hp-adaptive meshfree method and by Melenk and Babuška (1996) in a Partition-of-Unity Finite-Element Method. Subsequent to the introduction of discontinuous enrichment functions for modeling crack growth by Belytschko and Black (1999), many new extensions and applications have been examined using the X-FEM. The coupling of the method with the Level-Set Method (LSM) was first proposed by Sukumar et al. (2001) to represent the geometry of stationary voids and material interfaces independently of the finite element mesh. The basic concepts were later adapted to the simulation of evolving phase interfaces by Merle and Dolbow (2002), Ji et al. (2002), and Chessa et al. (2002). An analogous method, using non-conforming basis functions, was also proposed by Rao et al. (2000). The coupling of the two methods facilitates the simulation of an evolving interface using the enrichment functions to capture the local solution and the level-set function to implicitly represent the geometry of the interface; no remeshing is required.

In this work, we present a methodology to investigate unstable interfacial evolution in SRHs with the XFE/LSM. The strategy extends many of the concepts introduced by Dolbow et al. (2004) to multi-dimensional problems, with a number of important modifications. One of the critical issues concerns the coupling of the primary fields—the motion and the diffusion potential—through the normal configurational force balance. Previously, we neglected transition kinetics on the interface, and used a Lagrange multiplier to enforce the resulting Dirichlet constraint for the diffusion potential. The multiplier was subsequently interpreted to extract the jump, across the interface, of the normal component of the solute flux. Subequently, we have identified a number of concerns with such an approach, particularly with regard to the simulation of unstable interface evolution. First, constructing approximation spaces for the primary fields and the multiplier satisfying an inf-sup, Babuška–Brezzi stability condition (Babuška, 1973) is not trivial. As discussed by Ji and Dolbow (2004), the most convenient choice for the space of multipliers does not appear to satisfy the inf-sup condition, whereby oscillations in the multipliers are triggered. Second, when computed via direct evaluation of the mechanical fields on the interface, the mechanical driving traction generally exhibits oscillations. Those oscillations are not associated with a lack of stability in the mechanical problem but, rather, are a direct consequence of allowing the interface to be oriented arbitrarily with respect to the underlying mesh. While enrichment does improve the approximation properties in the vicinity of the interface, it does not impart any additional smoothness to the basis.

Recently, there has been considerable attention devoted to the development of robust techniques for extracting discrete configurational forces from finite-element solutions. See, for example, the techniques discussed by Steinmann et al. (2001) and Mueller et al. (2002), which lead to expressions for "material point forces" at finite-element nodes residing on an interface, crack front, or other defect. Since those techniques are specific to finite-element meshes that explicitly fit the geometry of the singularities under

consideration, their adaptation to allow an enriched approximation and an interface of arbitrary geometry does not appear straightforward. The techniques used by Steinmann et al. (2001) and Mueller et al. (2002) do, however, have much in common with the widely-used domain-integral methods introduced by Li et al. (1985) and those methods have been implemented with the X-FEM to extract energy release rates along crack fronts.

In this paper, we present a theory which accounts for the role of interface propagation in the chemo-mechanical swelling of hydrogels. In so doing, we adopt the perspective of Gibbs (1878), who modeled phase interfaces as surfaces across which the material properties of the bulk phases may suffer discontinuities and, to account for localized interactions between phases, endowed these surfaces with excess fields. Our theory closely resembles a theory developed by Gurtin and Voorhees (1993) for diffusional phase transitions in crystalline solids. Of key importance is an interfacial equation, expressing configurational force balance (Gurtin and Struthers, 1990; Gurtin, 1995; Gurtin, 2000), which generalizes the Gibbs–Thomson relation arising in descriptions of alloy solidification (cf., e.g., Mullins and Sekerka (1963)) and supplements the conventional equations which express mass balance and standard force balance in the bulk phases and across the interface. Whereas the role of dissipative transition kinetics was neglected from our previous work (Dolbow et al., 2004), we account here for that effect.

On the numerical side, we adapt the domain integral method to extract the mechanical driving traction at the phase interface. Importantly, in the algorithmic setting our adaptation does not require the specification of an arbitrary domain size. Because the method also recasts surface-based quantities to volume-based quantities, it effectively smoothes any oscillations in the driving traction. We use similar techniques to represent the interfacial normal and total curvature, as well as to extract the jump in the normal component of the solute flux. Finally, we find that the introduction of dissipative transition kinetics leads to a physically-based regularization of the theory, a regularization which makes it possible to impose a weak statement of the normal configurational force balance without recourse to a mixed formulation.

The paper is organized as follows. The next Section details important theoretical developments for our sharp interface model of SRH kinetics. Section 3 provides a complete development of the theory, which extends that used by Dolbow et al. (2004) to account for dissipative interfacial kinetics. The representation of the interface with level sets and the variational formulation are described in Sections 4 and 5, respectively. Sections 6 and 7 describe the discretization with the hybrid XFE/LSM, including the domain-integral techniques. The solution strategy is described in Section 8, and a number of benchmark studies and investigations into unstable interface growth are provided in Section 9. Finally, a summary and concluding remarks are given in the last Section.

2 Background

Our approach to the basic theory follows closely that of Gurtin and Voorhees (1993), the major difference being that, to account for the extreme distortions that occur during the swelling of hydrogels, we allow for finite strains.

2.1 Kinematics

We consider a two-phase body identified with a bounded region $\mathcal{R}$ of three-dimensional Euclidean point space that it occupies in a fixed reference configuration. Labeling the swelled and collapsed phases by α and β, respectively, we assume that for each time

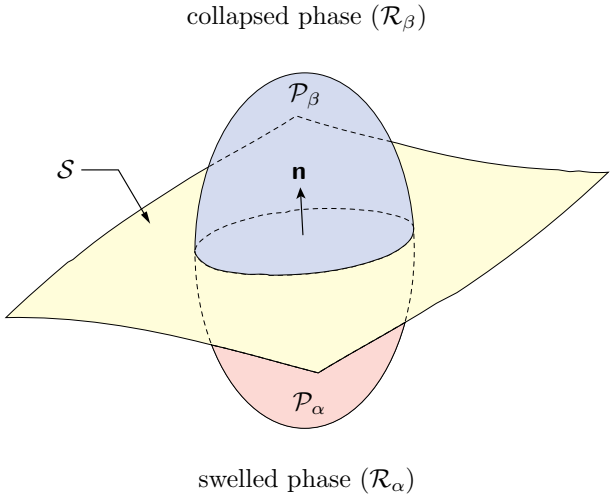

Figure 1: Schematic indicating: portions of the regions occupied by the swelled and collapsed phases; the evolving interface $\mathcal{S}$, with unit normal $\mathbf{n}$ directed into the collapsed phase; a fixed control volume $\mathcal{P}$, with outward unit normal $\mathbf{m}$, divided by $\mathcal{S}$ into time-dependent regions $\mathcal{P}_\alpha$ and $\mathcal{P}_\beta$ in the swelled and collapsed phases; and the portion $\mathcal{Q} = \mathcal{P} \cap \mathcal{S}$ of $\mathcal{S}$, with outward unit normal $\mathbf{m}$ tangent to $\mathcal{S}$, contained within $\mathcal{P}$.

t: $\mathcal{R}$ is separated by an interface $\mathcal{S}(t)$ into complementary subregions $\mathcal{R}_\alpha(t)$ and $\mathcal{R}_\beta(t)$ occupied by phases α and β.

We assume that $\mathcal{S}$ is a smoothly evolving surface oriented by a unit normal field $\mathbf{n}$, directed outward from $\mathcal{R}_\alpha$ (Figure 1). An interfacial field is a smooth field defined on $\mathcal{S}$ for all time. An interfacial vector field $\mathbf{g}$ is tangential if $\mathbf{g}\cdot\mathbf{n} = 0$. For an interfacial tensor field $\mathbf{H}$ we require that

$$\mathbf{H}\mathbf{n} = \mathbf{0}; \tag{2.1}$$

if, in addition, $\mathbf{H}^\top\mathbf{n} = \mathbf{0}$, we then say that $\mathbf{H}$ is fully tangential, so that $\mathbf{H}$ maps tangent vectors into tangent vectors. An example of a fully tangential tensor field is the interfacial projector

$$\mathbf{P} = \mathbf{I} - \mathbf{n}\otimes\mathbf{n}. \tag{2.2}$$

Each interfacial tensor field $\mathbf{H}$ admits a decomposition of the form

$$\mathbf{H} = \mathbf{H}_{\rm tan} + \mathbf{n}\otimes\mathbf{h}, \tag{2.3}$$

in which $\mathbf{H}_{\rm tan} = \mathbf{P}\mathbf{H}$ is fully tangential and $\mathbf{h} = \mathbf{H}^\top\mathbf{n}$ is tangential.

The interfacial field defined by

$$\mathsf{K} = -{\rm Div}_{\mathcal{S}}\mathbf{n} \tag{2.4}$$

is the *total* (i.e., twice the mean) *curvature* of $\mathcal{S}$. By (2.2), we then have the identity

$${\rm Div}_{\mathcal{S}}\mathbf{P} = \mathsf{K}\mathbf{n}. \tag{2.5}$$

We write v for the (scalar) *normal velocity* of $\mathcal{S}$. Let g be a field on $\mathcal{S}$. Given any time t_0 and any point $\mathbf{x}_0$ on $\mathcal{S}(t_0)$, let $\mathbf{z}$ denote the unique solution of

$$\frac{d\mathbf{z}(t)}{dt} = \mathbf{v}(\mathbf{z}(t), t), \qquad \mathbf{z}(t_0) = \mathbf{x}_0, \tag{2.6}$$

and define

$$\overset{\square}{\mathsf{g}}(\mathbf{x}_0, t_0) = \left.\frac{d\mathsf{g}(\mathbf{z}(\mathsf{t}), \mathsf{t})}{dt}\right|_{t=t_0}. \tag{2.7}$$

The field $\overset{\square}{\mathsf{g}}$ defined in this manner is referred to as the normal time-derivative of g following $\mathcal{S}$. The normal time-derivative $\overset{\square}{\mathbf{n}}$ of the orientation $\mathbf{n}$ and the scalar normal-velocity v are then related by the identity

$$\overset{\square}{\mathbf{n}} = -\mathrm{Grad}_{\mathcal{S}}\mathsf{v}. \tag{2.8}$$

Also important in what follows is the interfacial transport theorem (Gurtin, 1995): for g a smooth superficial scalar field,

$$\overset{\cdot}{\int_{\mathcal{Q}} \mathsf{g}\, da} = \int_{\mathcal{Q}} (\overset{\square}{\mathsf{g}} - \mathsf{g}\mathsf{K}\mathsf{v})\, da + \int_{\partial\mathcal{Q}} \mathsf{g}\mathsf{w}\, dl. \tag{2.9}$$

We assume that each bulk field is smooth up to $\mathcal{S}$ from either phase. We write

$$[\![\Phi]\!] \qquad \text{and} \qquad \langle\!\langle \Phi \rangle\!\rangle \tag{2.10}$$

for the jump and average of a bulk field Φ across $\mathcal{S}$: $[\![\Phi]\!]$ is the interfacial limit of Φ from the phase β (the phase into which $\mathbf{n}$ points) minus its limit from the phase α; $\langle\!\langle \Phi \rangle\!\rangle$ is the average value of these two limits.

We write $\mathbf{y}$ for the motion of the body. Basic to the theory is the assumption of coherence,

$$[\![\mathbf{y}]\!] = \mathbf{0}, \tag{2.11}$$

which requires that the motion be continuous across the phase interface. Introducing the deformation gradient $\mathbf{F} = \mathrm{Grad}\,\mathbf{y}$ and the velocity $\dot{\mathbf{y}}$, we have, as consequences of (2.11), the compatibility conditions

$$[\![\mathbf{F}]\!]\mathbf{P} = \mathbf{0} \qquad \text{and} \qquad [\![\dot{\mathbf{y}}]\!] + [\![\mathbf{F}]\!]\mathbf{v} = \mathbf{0}. \tag{2.12}$$

Motivated by (2.11), we introduce the interfacial deformation $\mathbf{y} = \mathbf{y}|_{\mathcal{S}}$ and deformation gradient

$$\mathbf{F} = \mathrm{Grad}_{\mathcal{S}}\mathbf{y}. \tag{2.13}$$

Direct calculations based on the compatibility conditions (2.12) then show that

$$\mathbf{F} = \mathbf{A}\mathbf{P} \qquad \text{and} \qquad \overset{\square}{\mathbf{y}} = \langle\!\langle \dot{\mathbf{y}} \rangle\!\rangle + \mathbf{A}\mathbf{v}, \tag{2.14}$$

with

$$\mathbf{A} = \langle\!\langle \mathbf{F} \rangle\!\rangle \tag{2.15}$$

the interfacial average of the deformation gradient.

2.2 Mechanics

In addition to deformational forces associated with the motion of material particles, we account for configurational forces (Gurtin and Struthers, 1990; Gurtin, 1995; Gurtin, 2000) associated with the motion of the nonmaterial interface separating the swelled and collapsed phases. We neglect inertia and all other external body forces.

To state the fundamental balances, we use an arbitrary fixed control-volume $\mathcal{P}$ with outward unit normal $\mathbf{m}$, as depicted in Figure 1. Further, writing $\mathcal{Q}(t) = \mathcal{P} \cap \mathcal{S}(t)$ for the (possibly empty) portion of the interface that lies within $\mathcal{P}$ at time t, we use $\mathbf{m}$ and w to denote the unit normal and tangential edge-velocity of $\partial\mathcal{Q}$.

2.2.1 Deformational force and moment balance

Since we neglect external force, the deformational force system consists only of the bulk deformational stress $\mathbf{S}$ and the interfacial deformational stress S. The balances of deformational forces and moment balances therefore require that

$$\int_{\partial\mathcal{P}} \mathbf{S}\mathbf{m}\, da + \int_{\partial\mathcal{Q}} \mathsf{S}\mathbf{m}\, dl = \mathbf{0} \tag{2.16}$$

and

$$\int_{\partial\mathcal{P}} \mathbf{y}\times\mathbf{S}\mathbf{m}\, da + \int_{\partial\mathcal{Q}} \mathbf{y}\times\mathsf{S}\mathbf{m}\, dl = \mathbf{0} \tag{2.17}$$

for all $\mathcal{P}$ and all time. These imply the bulk equations

$$\operatorname{Div}\mathbf{S} = \mathbf{0} \qquad \text{and} \qquad \mathbf{S}\mathbf{F}^{\top} = \mathbf{F}\mathbf{S}^{\top} \tag{2.18}$$

and the interfacial equations

$$[\![\mathbf{S}]\!]\mathbf{n} + \operatorname{Div}_s\mathsf{S} = \mathbf{0} \qquad \text{and} \qquad \mathsf{S}\mathbf{F}^{\top} = \mathsf{F}\mathsf{S}^{\top}. \tag{2.19}$$

2.2.2 Configurational force balance

The configurational force system consists of a bulk configurational stress $\mathbf{C}$, a bulk configurational force density $\mathbf{f}$, an superficial configurational stress C, and an superficial configurational force density f. We assume that these fields comply with the configurational force balance

$$\int_{\partial\mathcal{P}} \mathbf{C}\mathbf{m}\, da + \int_{\mathcal{P}} \mathbf{f}\, dv + \int_{\partial\mathcal{Q}} \mathsf{C}\mathbf{m}\, dl + \int_{\mathcal{Q}} \mathsf{f}\, da = \mathbf{0} \tag{2.20}$$

for all $\mathcal{P}$ and all time. This implies the bulk equation

$$\operatorname{Div}\mathbf{C} + \mathbf{f} = \mathbf{0} \tag{2.21}$$

and the interfacial equation

$$[\![\mathbf{C}]\!]\mathbf{n} + \operatorname{Div}_s\mathsf{C} + \mathsf{f} = \mathbf{0}. \tag{2.22}$$

Applying the decomposition (2.3) to C and introducing the normal internal force

$$\mathsf{f} = \mathbf{f}\cdot\mathbf{n}, \tag{2.23}$$

we obtain from (2.22) the normal configurational force balance

$$\mathbf{n}\cdot[\![\mathbf{C}]\!]\mathbf{n} + \mathsf{C}_{\tan}\cdot\mathsf{L} + \operatorname{Div}_s\mathsf{c} + \mathsf{f} = 0, \tag{2.24}$$

which is of central importance in the theory.

2.3 Solute balance

We treat the polymer chains as a solute with concentration c and flux $\mathbf{j}$. Neglecting diffusion within the interface, solute balance is the requirement that

$$\overset{\cdot}{\int_{\mathcal{P}} c\, dv} = -\int_{\partial\mathcal{P}} \mathbf{j}\cdot\mathbf{m}\, da \tag{2.25}$$

for all $\mathcal{P}$ and all time. This implies bulk equation

$$\dot{c} = -\mathrm{Div}\mathbf{j} \tag{2.26}$$

and the interfacial equation

$$\mathsf{v}[\![c]\!] = [\![\mathbf{j}]\!]\cdot\mathbf{n}. \tag{2.27}$$

2.4 Energetics

2.4.1 Free-energy

Introducing the bulk free-energy density Ψ and the interfacial free-energy density Ψ, the net free-energy of $\mathcal{P}$ is

$$\int_{\mathcal{P}} \Psi \, dv + \int_{\mathcal{Q}} \Psi \, da. \tag{2.28}$$

Further, the integral

$$-\int_{\partial\mathcal{Q}} \Psi\mathsf{w} \, dl \tag{2.29}$$

represents the rate at which free-energy is carried into $\mathcal{Q}$ by the motion of $\mathcal{S}$.

2.4.2 Diffusion potential. Free-energy inflow due to solute transport

To account for changes in free energy associated with solute transport, we introduce the diffusion potential u, which measures the chemical potential of the polymer chains with respect to that of the solvent. The integral

$$-\int_{\partial\mathcal{P}} u\mathbf{j}\cdot\mathbf{m} \, da \tag{2.30}$$

then represents the free-energy carried into $\mathcal{P}$ by the transport of solute across $\partial\mathcal{P}$. Basic to our theory is the assumption of local chemical equilibrium,

$$[\![u]\!] = 0, \tag{2.31}$$

which requires that the diffusion potential be continuous across the interface.

2.4.3 Power

The power expended on $\mathcal{P}$ must account not only for the working of the deformational traction $\mathbf{Sm}$ distributed over the boundary $\partial\mathcal{P}$ of the control volume, but also for the workings of the deformational traction $\mathbf{Sm}$ and the configurational traction $\mathbf{Cm}$ distributed over the curve $\partial\mathcal{Q}$ formed by the intersection of the interface $\mathcal{S}$ with $\partial\mathcal{P}$. As a material surface, $\mathcal{P}$ may be described intrinsically in terms of the motion. The traction $\mathbf{Sm}$ is therefore power-conjugate to the material velocity $\dot{\mathbf{y}}$. By analogy, we expect that the interfacial deformational traction $\mathbf{Sm}$ should be power-conjugate to the motion velocity $\overset{\square}{\mathbf{y}}$ following the interface. On the other hand, the configurational traction $\mathbf{Cm}$ is associated with the change in material structure accompanying the evolution of the phase interface and is thus power-conjugate to the intrinsic velocity $\mathbf{v} = \mathsf{v}\mathbf{n}$ of the interface (Gurtin and Struthers, 1990; Gurtin, 1995; Gurtin, 2000). Thus, bearing in mind

that $\mathcal{P}$ is fixed (whereby there is no working associated with the configurational traction $\mathbf{Cm}$ over $\partial\mathcal{P}$), it follows that the total power expended on $\mathcal{P}$ by external agencies is $\int_{\partial\mathcal{P}} \mathbf{Sm}\cdot\dot{\mathbf{y}}\,da + \int_{\partial\mathcal{Q}} \left(\mathbf{Sm}\cdot\dot{\overset{\square}{\mathbf{y}}} + \mathbf{Cm}\cdot\mathbf{v}\right) dl$, which, in view of the decomposition $\mathbf{C} = \mathbf{C}_{\rm tan} + \mathbf{n}\otimes\mathbf{c}$ of the interfacial configurational stress, can be written alternatively as

$$\int\limits_{\partial\mathcal{P}} \mathbf{Sm}\cdot\dot{\mathbf{y}}\,da + \int\limits_{\partial\mathcal{Q}} \left(\mathbf{Sm}\cdot\dot{\overset{\square}{\mathbf{y}}} + \mathbf{c}\cdot(\mathsf{v}\mathbf{m})\right) dl. \tag{2.32}$$

2.4.4 Free-energy imbalance

We confine our attention to isothermal circumstances. The first and second laws of thermodynamics then combine to yield a free-energy imbalance requiring that, for each control volume $\mathcal{P}$ and each time, the rate of change of the free energy of $\mathcal{P}$ not exceed the sum of the energy carried into $\mathcal{P}$ by bulk diffusion across its boundary and the power expended on $\mathcal{P}$ by external agencies. Bearing in mind (2.29), (2.30), and (2.32), free-energy imbalance is the requirement that

$$\dot{\overline{\int\limits_{\mathcal{P}} \Psi\,dv + \int\limits_{\mathcal{Q}} \Psi\,da}} - \int\limits_{\partial\mathcal{Q}} \Psi\mathsf{w}\,dl \leq -\int\limits_{\partial\mathcal{P}} u\mathbf{j}\cdot\mathbf{m}\,da + \int\limits_{\partial\mathcal{P}} \mathbf{Sm}\cdot\dot{\mathbf{y}}\,da + \int\limits_{\partial\mathcal{Q}} (\mathbf{Sm}\cdot\dot{\overset{\square}{\mathbf{y}}} + (\mathbf{c}\cdot\mathbf{m})\mathsf{v})\,dl \tag{2.33}$$

for all $\mathcal{P}$ and all time. In view of the interfacial transport theorem (2.9), the bulk balances $(2.18)_1$ and (2.26), the kinematic relation $(2.4)_2$, (2.8), $(2.12)_2$, and $(2.14)_2$, the commutator identity

$$\mathrm{Grad}_{\mathcal{S}}\dot{\overset{\square}{\mathbf{y}}} = \dot{\overset{\square}{\mathbf{F}}} + \mathbf{F}\dot{\overset{\square}{\mathbf{n}}}\otimes\mathbf{n} - \mathsf{v}\mathbf{F}\mathbf{L} = \dot{\overset{\square}{\mathbf{A}}}\mathbf{P} - \mathbf{A}\mathbf{n}\otimes\dot{\overset{\square}{\mathbf{n}}} - \mathsf{v}\mathbf{F}\mathbf{L} \tag{2.34}$$

(Gurtin, 2000), and the interfacial balances $(2.19)_1$, (2.24), and (2.27), (2.33) implies bulk free-energy inequality

$$\dot{\Psi} - u\dot{c} - \mathbf{S}\cdot\dot{\mathbf{F}} + \mathbf{j}\cdot\mathrm{Grad}\,u \leq 0 \tag{2.35}$$

and the interfacial free-energy inequality

$$\dot{\overset{\square}{\Psi}} - \mathbf{S}\cdot\dot{\overset{\square}{\mathbf{A}}} + \mathbf{p}\cdot\dot{\overset{\square}{\mathbf{n}}} + (\mathsf{f} + \mathbf{n}\cdot[\![\mathbf{D}]\!]\mathbf{n} + \mathbf{D}\cdot\mathbf{L})\mathsf{v} \leq 0, \tag{2.36}$$

where we have introduced

$$\mathbf{p} = \mathbf{c} + \mathbf{S}^{\top}\mathbf{A}\mathbf{n}, \quad \mathbf{D} = \mathbf{C} - (\Psi - cu)\mathbf{I} + \mathbf{F}^{\top}\mathbf{S}, \quad \text{and} \quad \mathbf{D} = \mathbf{C}_{\rm tan} - \Psi\mathbf{P} + \mathbf{F}^{\top}\mathbf{S}. \tag{2.37}$$

2.5 Eshelby relations

If, following Gurtin (1995, 2000), we consider the free-energy imbalance for a migratrating control-volume, the requirement that the imbalance be invariant under changes of parameterization of the boundary of that volume implies that the bulk configurational stress be given by the classical Eshelby relation

$$\mathbf{C} = (\Psi - cu)\mathbf{I} - \mathbf{F}^{\top}\mathbf{S} \tag{2.38}$$

and that the tangential component $\mathbf{C}_{\rm tan}$ of the interfacial configurational stress $\mathbf{C}$ be given by the analogous interfacial Eshelby relation

$$\mathbf{C}_{\rm tan} = \Psi\mathbf{P} - \mathbf{F}^{\top}\mathbf{S}. \tag{2.39}$$

In view of (2.38) and (2.39), $\mathbf{D}$ and $\mathbf{D}$ as defined in $(2.37)_2$ vanish and the interfacial free-energy inequality (2.36) reduces to

$$\dot{\overset{\square}{\Psi}} - \mathbf{S}\cdot\dot{\overset{\square}{\mathbf{A}}} + \mathbf{p}\cdot\dot{\overset{\square}{\mathbf{n}}} + \mathsf{f}\mathsf{v} \leq 0, \tag{2.40}$$

2.6 Constitutive equations

2.6.1 Bulk constitutive equations

Our framework for bulk constitutive equations follows those presented by Gurtin and Voorhees (1993) and Fried and Gurtin (1999), excepting that we account for finite strains. Introducing the canonical-energy density

$$\Omega = \Psi - cu, \tag{2.41}$$

we rewrite the bulk free-energy inequality (2.35) as

$$\dot{\Omega} + c\dot{u} - \mathbf{S}\cdot\dot{\mathbf{F}} + \mathbf{j}\cdot\operatorname{Grad} u \leq 0. \tag{2.42}$$

Consistent with the isotropy of gel-like substances, we assume that Ω, $\mathbf{S}$, c and $\mathbf{j}$ are determined constitutively by isotropic functions of the left Cauchy–Green tensor $\mathbf{B} = \mathbf{F}\mathbf{F}^{\top}$, u, and $\operatorname{Grad} u$. In particular, introducing the principal invariants

$$I_1(\mathbf{B}) = \operatorname{tr}\mathbf{B}, \quad I_2(\mathbf{B}) = \tfrac{1}{2}(I_1^2(\mathbf{B}) - I_1(\mathbf{B}^2)), \quad \text{and} \quad I_3(\mathbf{B}) = \det\mathbf{B} \tag{2.43}$$

of $\mathbf{B}$ and writing

$$\imath(\mathbf{B}) = (I_1(\mathbf{B}), I_2(\mathbf{B}), I_3(\mathbf{B})), \tag{2.44}$$

we assume that, in each phase $\gamma = \alpha, \beta$,

$$\left.\begin{aligned} \Omega = \Omega_\gamma(\imath(\mathbf{B}), u), \qquad \mathbf{S} = \frac{\partial\Omega_\gamma(\imath(\mathbf{B}), u)}{\partial\mathbf{F}}, \qquad c = -\frac{\partial\Omega_\gamma(\imath(\mathbf{B}), u)}{\partial u}, \\ \mathbf{j} = -\mathbf{M}^\gamma(\imath(\mathbf{B}), u)\operatorname{Grad} u, \end{aligned}\right\} \tag{2.45}$$

with

$$\mathbf{M}^\gamma(\imath(\mathbf{B}), u) = \hat{M}_0^\gamma(\imath(\mathbf{B}), u)\mathbf{I} + \hat{M}_1^\gamma(\imath(\mathbf{B}), u)\mathbf{B} + \hat{M}_2^\gamma(\imath(\mathbf{B}), u)\mathbf{B}^2) \tag{2.46}$$

and

$$\hat{M}_0^\gamma(\imath(\mathbf{B}), u)|\mathbf{g}|^2 + \hat{M}_1^\gamma(\imath(\mathbf{B}), u)|\mathbf{F}^{\top}\mathbf{g}|^2 + \hat{M}_2^\gamma(\imath(\mathbf{B}), u)|\mathbf{B}\mathbf{g}|^2 > 0 \qquad \text{for all } \mathbf{g}. \tag{2.47}$$

2.6.2 Interfacial constitutive equations

Consistent with the isotropy of gel-like substances, we neglect constitutive dependence on n and assume that $\mathsf{\Psi}$, S, p, and f are determined constitutively by isotropic functions of $\mathsf{A}\mathsf{A}^{\top}$ and v. It follows that the inequality (2.40) holds if and only if

$$\mathsf{\Psi} = \tilde{\mathsf{\Psi}}(\imath(\mathsf{A}\mathsf{A}^{\top})), \quad \mathsf{S} = \frac{\partial\tilde{\mathsf{\Psi}}(\imath(\mathsf{A}\mathsf{A}^{\top}))}{\partial\mathsf{A}}, \quad \mathsf{p} = \mathbf{0}, \quad \text{and} \quad \mathsf{f} = -\mathsf{b}(\imath(\mathsf{A}\mathsf{A}^{\top}), \mathsf{v})\mathsf{v}, \tag{2.48}$$

where b must satisfy

$$\mathsf{b}(\imath(\mathsf{A}\mathsf{A}^{\top}), \mathsf{v}) \geq 0. \tag{2.49}$$

2.7 Evolution equations

Combining the bulk constitutive equations (2.45) with the bulk deformational force balance $(2.18)_1$ and mass balance (2.26) yields equations,

$$\left.\begin{aligned} \operatorname{Div}\left(\frac{\partial \Omega_\gamma(\imath(\mathbf{B}),u)}{\partial \mathbf{F}}\right)&=\mathbf{0},\\ \dot{\overline{\frac{\partial \Omega_\gamma(\imath(\mathbf{B}),u)}{\partial u}}}&=-\operatorname{Div}\left(\mathbf{M}_\gamma(\imath(\mathbf{B}),u)\operatorname{Grad} u\right),\end{aligned}\right\} \tag{2.50}$$

on the evolving regions $\mathcal{R}_\gamma$ occupied by the bulk phases $\gamma=\alpha,\beta$. Similarly, combining the bulk and interfacial constitutive equations (2.45), and (2.48) with the interfacial deformational force balance $(2.19)_1$ and mass balance (2.27) yields equations,

$$\left.\begin{aligned} \left[\!\left[\frac{\partial \Omega_\gamma(\imath(\mathbf{B}),u)}{\partial \mathbf{F}}\right]\!\right]\mathbf{n}+\operatorname{Div}_{\mathcal{S}}\left(\frac{\partial \tilde{\Psi}(\imath(\mathbf{A}\mathbf{A}^{\top})}{\partial \mathbf{A}}\right)&=\mathbf{0},\\ \mathsf{v}\left[\!\left[\frac{\partial \Omega_\gamma(\imath(\mathbf{B}),u)}{\partial u}\right]\!\right]&=\left[\!\left[\mathbf{M}_\gamma(\imath(\mathbf{B}),u)\operatorname{Grad} u\right]\!\right]\cdot\mathbf{n},\end{aligned}\right\} \tag{2.51}$$

on the evolving phase interface $\mathcal{S}$. The normal configurational force balance (2.24) yields an additional evolution equation,

$$\begin{aligned}\mathbf{n}\cdot\left[\!\left[\Omega_\gamma(\imath(\mathbf{B}),u)\mathbf{I}-\mathbf{F}^{\top}\frac{\partial \Omega_\gamma(\imath(\mathbf{B}),u)}{\partial \mathbf{F}}\right]\!\right]\mathbf{n}+\left(\tilde{\Psi}(\mathbf{A})\mathbf{P}-\mathbf{F}^{\top}\frac{\partial \tilde{\Psi}(\imath(\mathbf{A}\mathbf{A}^{\top})}{\partial \mathbf{A}}\right)\cdot\mathbf{L}\\ +\operatorname{Div}_{\mathcal{S}}\left(\left(\frac{\partial \tilde{\Psi}(\imath(\mathbf{A}\mathbf{A}^{\top})}{\partial \mathbf{A}}\right)^{\top}\mathbf{A}\mathbf{n}\right)=\mathsf{b}(\imath(\mathbf{A}\mathbf{A}^{\top},\mathsf{v})\mathsf{v},\end{aligned} \tag{2.52}$$

on $\mathcal{S}$. Here, consistent with the convention that $\mathbf{n}$ points into $\mathcal{R}_\beta$, $[\![g_\gamma]\!]=g_\beta-g_\alpha$. The interface conditions (2.51) and (2.52) are supplemented by the conditions (2.11) of coherency and (2.31) and local equilibrium.

Missing from the foregoing list of equations are the bulk and interfacial moment balances $(2.18)_2$ and $(2.19)_2$, the bulk configurational force balance (2.21), and the tangential component of the interfacial configurational force balance (2.22). Implicit to (2.45) and (2.48) is the requirement that the constitutive response functions be properly invariant under superposed rigid motions; the bulk and interfacial moment balances $(2.18)_2$ and $(2.19)_2$ are therefore satisfied and may be removed from further consideration. Because it does not appear in the free-energy inequality (2.35), the bulk configurational force $\mathbf{f}$ cannot be determined independently via a constitutive relation. Instead, that force is assigned to ensure satisfaction of the bulk configurational force balance (2.21); thus, $\mathbf{f}=-\operatorname{Div}\mathbf{C}$. To determine the form of $\mathbf{f}$, we use the constitutive relations (2.45) in the bulk Eshelby relation (2.38) and compute $\operatorname{Div}\mathbf{C}$. By the bulk deformational force balance (2.50), it follows that $\operatorname{Div}\mathbf{C}=-c\operatorname{Grad}u$ and, thus, that $\mathbf{f}=c\operatorname{Grad}u$. Hence, $\mathbf{f}$ vanishes when the diffusion potential is uniform. The role of the tangential component $\mathbf{f}_{\tan}=\mathbf{f}-\mathsf{f}\mathbf{n}$ of the interfacial configurational force $\mathbf{f}$ is analogous to that of $\mathbf{f}$. Being absent from the free-energy inequality (2.40), $\mathbf{f}_{\tan}$ is assigned to ensure satisfaction of the tangential component of the interfacial configurational force balance (2.22); thus $\mathbf{f}_{\tan}=-\mathbf{P}([\![\mathbf{C}]\!]\mathbf{n}+\operatorname{Div}_{\mathcal{S}}\mathbf{C})$. To determine the form of $\mathbf{f}_{\tan}$, we use the definition $(2.37)_1$ of $\mathbf{p}$ and the constitutive relations (2.45) and $(2.48)_{1,2,3}$ in the bulk and interfacial Eshelby relations (2.38) and (2.22) to compute $[\![\mathbf{C}]\!]\mathbf{n}+\operatorname{Div}_{\mathcal{S}}\mathbf{C}$. By the interfacial deformational force balance (2.19), it follows that $\mathbf{P}([\![\mathbf{C}]\!]\mathbf{n}+\operatorname{Div}_{\mathcal{S}}\mathbf{C})=\mathbf{0}$ and, thus, that $\mathbf{f}_{\tan}=\mathbf{0}$.

2.8 Boundary conditions

Writing $\boldsymbol{\nu}$ for the unit orientation of $\partial\mathcal{R}$, directed outward from $\mathcal{R}$, we assume that

$$\mathbf{y}|_{(\partial\mathcal{R})_{\mathrm{m}}} = \bar{\mathbf{y}} \qquad \text{and} \qquad (\mathbf{S}\boldsymbol{\nu})|_{(\partial\mathcal{R})_{\mathrm{t}}} = \mathbf{s}, \tag{2.53}$$

with $(\partial\mathcal{R})_{\mathrm{m}}$ and $(\partial\mathcal{R})_{\mathrm{t}}$ complementary subsets of $\partial\mathcal{R}$, and that

$$u|_{(\partial\mathcal{R})_{\mathrm{p}}} = \bar{u} \qquad \text{and} \qquad (\mathbf{j}\cdot\boldsymbol{\nu})|_{(\partial\mathcal{R})_{\mathrm{f}}} = j, \tag{2.54}$$

with $(\partial\mathcal{R})_{\mathrm{p}}$ and $(\partial\mathcal{R})_{\mathrm{f}}$ complementary subsets of $\partial\mathcal{R}$.

3 Specialization of the theory

Motivated by the experimental observations of Gehrke et al. (1992), we now specialize the theory to situations in which the time scale associated with the motion of the interface is slow with respect to that associated with diffusion in the bulk phases. Following Gurtin and Voorhees (1993), such a theory arises by restricting the canonical-energy density in each phase to be linear in u, viz.,

$$\Omega_\gamma(\imath(\mathbf{B}), u) = W_\gamma(\imath(\mathbf{B})) - c_\gamma u, \tag{3.1}$$

with c_γ constant. Consistent with the intuitive expectation that the solute concentration in the collapsed phase should exceed that in the swelled phase, we assume that

$$0 < c_\alpha < c_\beta < 1. \tag{3.2}$$

For simplicity, we assume that

$$\begin{aligned} W_\gamma(\imath(\mathbf{B})) = \frac{\mu_\gamma}{2}\left(I_1(\mathbf{B}) - 2J_\gamma^{\frac{2}{3}}\log\left(\frac{\sqrt{I_3(\mathbf{B})}}{J_\gamma}\right) - 3J_\gamma^{\frac{2}{3}}\right) \\ + \frac{\lambda_\gamma J_\gamma^{\frac{2}{3}}}{4}\left(\left(\frac{\sqrt{I_3(\mathbf{B})}}{J_\gamma} - 1\right)^2 + \log^2\left(\frac{\sqrt{I_3(\mathbf{B})}}{J_\gamma}\right)\right) + J_\gamma^{\frac{2}{3}} w_\gamma, \end{aligned} \tag{3.3}$$

with $\mu_\gamma > 0$ and $\lambda_\gamma > 0$ mechanical moduli for phase γ and w_γ constant. It can be shown that phase γ is stress-free at the energetically preferred dilatation $\mathbf{F} = J_\gamma\mathbf{I}$, and that μ_γ and λ_γ correspond to conventional shear and Lamé moduli for infinitesimal deviations about this stress-free state (Dolbow et al., 2004). The difference $J_\beta^{2/3}w_\beta - J_\alpha^{2/3}w_\alpha$ determines the energetic preference between the phases in their stress-free states. Without loss of generality, we take

$$J_\beta = 1. \tag{3.4}$$

Then, since α is the swelled phase, we must necessarily have

$$J_\alpha > 1. \tag{3.5}$$

In addition, we assume that

$$\mathbf{M}_\gamma(\imath(\mathbf{B}), u) = m_\gamma\mathbf{I}, \tag{3.6}$$

where m_γ is the constant (scalar) molecular mobility in phase γ and, by (2.47), consistent with

$$m_\gamma > 0. \tag{3.7}$$

Further, for simplicity, we assume that the interfacial free-energy density is constant

$$\tilde{\Psi}(\mathbf{A}) = \sigma, \tag{3.8}$$

so that $\mathbf{S} = \mathbf{0}$, and we incorporate transition kinetics by setting

$$\mathsf{b}(\mathbf{A}, \mathsf{v}) = \eta, \tag{3.9}$$

with $\eta > 0$ the constant reciprocal mobility of the interface.

Granted the constitutive specializations (3.1) and (3.6), (2.50) yields

$$\left.\begin{aligned} \mathrm{Div}\Big(\frac{\partial W_\gamma(\imath(\mathbf{B}))}{\partial \mathbf{F}}\Big) = \mathbf{0}, \\ m_\gamma \mathrm{Div}\,(\mathrm{Grad}\, u) = 0. \end{aligned}\right\} \tag{3.10}$$

Similarly, granted the constitutive specializations (3.8) and (3.9), (2.51) and (2.52) yield

$$\left.\begin{aligned} \Big[\!\Big[\frac{\partial W_\gamma(\imath(\mathbf{B}))}{\partial \mathbf{F}}\Big]\!\Big]\mathbf{n} = \mathbf{0}, \\ [\![c_\gamma]\!]\mathsf{v} + [\![m_\gamma \mathrm{Grad}\, u]\!]\cdot\mathbf{n} = 0, \\ [\![c_\gamma]\!]u + \eta\mathsf{v} = \sigma\mathsf{K} + \mathbf{n}\cdot[\![\mathbf{E}_\gamma(\mathbf{F})]\!]\mathbf{n}, \end{aligned}\right\} \tag{3.11}$$

where

$$\mathbf{E}_\gamma(\mathbf{F}) = W_\gamma(\imath(\mathbf{B}))\mathbf{I} - \mathbf{F}^\top \frac{\partial W_\gamma(\imath(\mathbf{B}))}{\partial \mathbf{F}} \tag{3.12}$$

denotes the mechanical contribution to the Eshelby tensor of phase γ.

The only explicit coupling between the fields $\mathbf{y}$ and u evident from (3.10) and (3.11) is through the normal configurational balance $(3.11)_3$.

4 Representation of the interface

We represent the interface as the zero-level set

$$\mathcal{S}(t) = \{\mathbf{x} : \zeta(\mathbf{x}, t) = 0\} \tag{4.1}$$

of a function ζ and, following Osher and Sethian (1988), insist that ζ satisfy

$$\dot{\zeta} + v^e |\mathrm{Grad}\,\zeta| = 0, \tag{4.2}$$

where the extension velocity v^e is constructed to obey

$$v^e|_{\zeta=0} = \mathsf{v}. \tag{4.3}$$

We take $\zeta > 0$ in the collapsed phase and $\zeta < 0$ in the swelled phase. The normal $\mathbf{n}$ and total curvature K of the interface can be expressed in terms of the function ζ via[1]

$$\mathbf{n} = \frac{\mathrm{Grad}\,\zeta}{|\mathrm{Grad}\,\zeta|} \qquad \text{and} \qquad \mathsf{K} = -\mathrm{Div}\left(\frac{\mathrm{Grad}\,\zeta}{|\mathrm{Grad}\,\zeta|}\right). \tag{4.4}$$

[1] The expression (4.4) for K is consistent with the definition (2.4) but does differ by a sign from the conventional choice the level-set literature.

5 Variational formulation

Throughout this section we suppress all dependence upon time.

5.1 Weak statement of the deformational force balance and normal interfacial force balance

We let $\mathcal{A}_{\rm m}$ denote the space of kinematically-admissible motions that are sufficiently regular and comply with the Dirichlet boundary condition $(2.53)_1$. Motions in $\mathcal{A}_{\rm m}$ automatically satisfy the coherency condition (2.11). We let $\mathcal{V}_{\rm m}$ denote the corresponding space of suitable variations with vanishing values on the essential boundary. Upon multiplying each term of the bulk force balance $(3.10)_1$ by an arbitrary weight function $\mathbf{w}$ in $\mathcal{V}_{\rm m}$, integrating the resulting equation over $\mathcal{R}\setminus\mathcal{S}$, and integrating by parts, we obtain the variational boundary-value-problem: find $\mathbf{y}$ in $\mathcal{A}_{\rm m}$ such that

$$\sum_{\gamma=\alpha,\beta}\int\limits_{\mathcal{R}_\gamma}\frac{\partial W_\gamma(\mathbf{F})}{\partial\mathbf{F}}\cdot\mathrm{Grad}\,\mathbf{w}\,dv=\int\limits_{(\partial\mathcal{R})_{\rm t}}\mathbf{s}\cdot\mathbf{w}\,da \tag{5.1}$$

for all variations $\mathbf{w}$ in $\mathcal{V}_{\rm m}$. In the derivation of the above, we have used the interfacial force balance $(3.11)_1$.

5.2 Weak statement of bulk solute balance, interfacial solute balance, and interfacial configurational force balance

We consider the space $\mathcal{A}_{\rm u}$ of sufficiently regular diffusion potentials satisfying the condition (2.31) of local chemical equilibrium and the Dirichlet boundary condition $(2.54)_1$. We use $\mathcal{V}_{\rm u}$ to denote the space of variations in the diffusion potential. Upon multiplying each term of the bulk solute balance $(3.10)_2$ by an arbitrary variation w in $\mathcal{V}_{\rm u}$, integrating the resulting equation over $\mathcal{R}\setminus\mathcal{S}$, and integrating by parts, we obtain

$$\sum_{\gamma=\alpha,\beta}\int\limits_{\mathcal{R}_\gamma}m_\gamma\mathrm{Grad}\,u\cdot\mathrm{Grad}\,w\,dv+\int\limits_{\mathcal{S}}[\![m_\gamma\mathrm{Grad}\,u]\!]\cdot\mathbf{n}\,w\,da=-\int\limits_{(\partial\mathcal{R})_{\rm f}}jw\,da. \tag{5.2}$$

Next, we eliminate the velocity v between the interfacial solute balance $(3.11)_2$ and the interfacial configurational balance $(3.11)_3$ to yield

$$[\![m_\gamma\mathrm{Grad}\,u]\!]\cdot\mathbf{n}=\frac{[\![c_\gamma]\!]}{\eta}\big([\![c_\gamma]\!]u-\mathbf{n}\cdot[\![\mathbf{E}_\gamma(\mathbf{F})]\!]\mathbf{n}-\sigma\mathsf{K}\big). \tag{5.3}$$

Finally, substituting (5.3) into (5.2) and rearranging terms, we obtain the variational boundary-value problem: find u in $\mathcal{A}_{\rm u}$ such that

$$\begin{aligned}\sum_{\gamma=\alpha,\beta}\int\limits_{\mathcal{R}_\gamma}m_\gamma\mathrm{Grad}\,u\cdot\mathrm{Grad}\,w\,dv+\frac{[\![c_\gamma]\!]^2}{\eta}\int\limits_{\mathcal{S}}uw\,da&\\ =-\int\limits_{(\partial\mathcal{R})_{\rm f}}jw\,da+\frac{[\![c_\gamma]\!]}{\eta}\int\limits_{\mathcal{S}}(\mathbf{n}\cdot[\![\mathbf{E}_\gamma(\mathbf{F})]\!]\mathbf{n}+\sigma\mathsf{K})w\,da&\end{aligned} \tag{5.4}$$

for all variations w in $\mathcal{V}_{\rm u}$. The above is equivalent to imposing the bulk and interfacial solute balances $(3.10)_2$ and $(3.11)_2$, the normal configurational force balance $(3.11)_3$, local chemical equilibrium (2.31), and the Dirichlet boundary condition $(2.54)_1$.

5.3 Domain integral approximations to interfacial quantities

We consider an arbitrary point $\mathbf{x}_\mathrm{d}$ on the interface where some interfacial quantity is desired. Let w_d denote a sufficiently smooth scalar-valued weight function w_d with compact support $\mathcal{B} = \mathrm{supp}(w_\mathrm{d})$ disjoint from $(\partial\mathcal{R})_\mathrm{n}$, so that $\mathcal{B} \cap (\partial\mathcal{R})_\mathrm{n} = \emptyset$, and containing $\mathbf{x}_\mathrm{d}$. We use $\mathcal{B}_\beta$ and $\mathcal{B}_\alpha$ to denote the intersection of $\mathcal{B}$ with $\mathcal{R}_\alpha$ and $\mathcal{R}_\beta$, respectively, and $\mathcal{L} = \mathcal{B} \cap \mathcal{S}$ to denote the portion of the interface that lies within $\mathcal{B}$ (Figure 2).

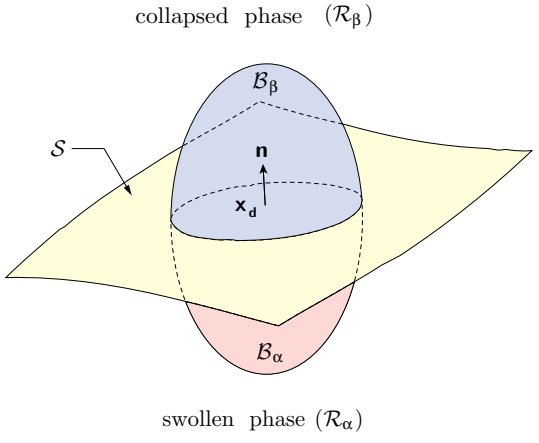

Figure 2: Local domain $\mathcal{B}$ corresponding to the support of a weight function w_d partitioned into complementary subsets $\mathcal{B}_\mathrm{s}$ and $\mathcal{B}_\mathrm{c}$ in the vicinity of point $\mathbf{x}_\mathrm{d}$ on the interface $\mathcal{S}$.

Consider, in particular, the mechanical driving traction

$$\mathsf{e} = \mathbf{n} \cdot [\![\mathbf{E}_\gamma(\mathbf{F})]\!] \mathbf{n}. \tag{5.5}$$

For $\mathbf{E}_\gamma(\mathbf{F})$ as defined by (3.12), it follows from the bulk deformational force balance $(3.10)_1$ that

$$\mathrm{Div}\, \mathbf{E}_\gamma(\mathbf{F}) = \mathbf{0} \tag{5.6}$$

on $\mathcal{R} \setminus \mathcal{S}$. Multiplying both sides of (5.6) by w_d, integrating the resulting equation over $\mathcal{R} \setminus \mathcal{S}$, and integrating by parts, we obtain

$$\sum_{\gamma=\alpha,\beta} \int\limits_{\mathcal{B}_\gamma} \mathbf{E}_\gamma(\mathbf{F}) \mathrm{Grad}\, w_\mathrm{d}\, dv = -\int\limits_{\mathcal{L}} [\![\mathbf{E}_\gamma(\mathbf{F})]\!] \mathbf{n}\, w_\mathrm{d}\, da. \tag{5.7}$$

Next, assuming that $[\![\mathbf{E}_\gamma(\mathbf{F})]\!] \mathbf{n}$ is constant over $\mathcal{L}$ and computing the dot product with the normal $\mathbf{n}$ at $\mathbf{x}_\mathrm{d}$, we obtain a simple approximate expression

$$\mathsf{e}(\mathbf{x}_\mathrm{d}) \approx -\frac{\left(\sum\limits_{\gamma=\alpha,\beta} \int\limits_{\mathcal{B}_\gamma} \mathbf{E}_\gamma(\mathbf{F}) \mathrm{Grad}\, w_\mathrm{d}\, dv \right) \cdot \mathbf{n}|_{\mathbf{x}_\mathrm{d}}}{\int\limits_{\mathcal{L}} w_\mathrm{d}\, da} \tag{5.8}$$

for the mechanical driving traction at $\mathbf{x}_\mathrm{d}$. Importantly, the calculation leading to (5.8) can be repeated for a sequence of local domains about selected points adjacent to the

interface and associated weight functions yielding an approximation for e at any point on the interface.

The expression (5.8) resembles domain forms of the J-integral and interaction integral designed to approximate the energy release rate at points along a three-dimensional crack front (see Shih et al. (1986) and Gosz et al. (1998)). These methods typically shift the divergence of the Eshelby tensor to the gradient of a weight function. The weight function is often referred to as the virtual crack extension and is constructed to vanish on the surface of the local domain enclosing the crack front. A first-order approximation, identical to that leading to (5.8), is then invoked to obtain pointwise values.

An alternative approximation to e takes advantage of the expression $(4.4)_1$ for the interface normal $\mathbf{n}$ in terms of the level-set function ζ. Since ζ is defined over the entire domain, $(4.4)_1$ may be viewed as an extension of the interface normal to points not on the interface, which we denote as $\mathbf{n}^e$. Computing the dot product of this extended normal with (5.6), multiplying each term of the resulting equation by $w_{\rm d}$, integrating over $\mathcal{R}\setminus\mathcal{S}$, and integrating by parts, we obtain

$$\int\limits_{\mathcal{L}} \mathsf{e} w_{\rm d}\, da = -\sum_{\gamma=\alpha,\beta} \int\limits_{\mathcal{B}_\gamma} \mathbf{n}^e\cdot\mathbf{E}_\gamma(\mathbf{F})\mathrm{Grad}\, w_{\rm d}\, dv - \sum_{\gamma=\alpha,\beta} \int\limits_{\mathcal{B}_\gamma} \mathrm{Grad}\,\mathbf{n}^e\cdot\mathbf{E}_\gamma(\mathbf{F}) w_{\rm d}\, dv. \tag{5.9}$$

Assuming that e is constant over $\mathcal{L}$, we obtain

$$\mathsf{e}(\mathbf{x}_{\rm d}) \approx -\frac{\displaystyle\sum_{\gamma=\alpha,\beta} \int\limits_{\mathcal{B}_\gamma} \mathbf{n}^e\cdot\mathbf{E}_\gamma(\mathbf{F})\mathrm{Grad}\, w_{\rm d}\, dv + \sum_{\gamma=\alpha,\beta} \int\limits_{\mathcal{B}_\gamma} \mathrm{Grad}\,\mathbf{n}^e\cdot\mathbf{E}_\gamma(\mathbf{F}) w_{\rm d}\, dv}{\displaystyle\int\limits_{\mathcal{L}} w_{\rm d}\, da}. \tag{5.10}$$

Whenever e is closer to constant over $\mathcal{L}$ than are the components of $[\![\mathbf{E}_\gamma(\mathbf{F})]\!]\mathbf{n}$, the approximation provided by (5.10) should be more accurate than that provided by (5.8).

Nearly any jump quantity of interest can be recast in the manner leading to (5.8), provided that a corresponding bulk relationship is identifiable. Consider, in particular, the jump

$$\mathsf{j} = [\![m_\gamma \mathrm{Grad}\, u]\!]\cdot\mathbf{n} \tag{5.11}$$

of the normal component of solute flux across the interface at point $\mathbf{x}_{\rm d}$. Upon multiplying each term of the *bulk* solute balance $(3.10)_2$ by $w_{\rm d}$, integrating the resulting equation over $\mathcal{B}$, and integrating by parts, we obtain

$$\sum_{\gamma=\alpha,\beta} \int\limits_{\mathcal{B}_\gamma} m_\gamma \mathrm{Grad}\, u\cdot\mathrm{Grad}\, w_{\rm d}\, dv = -\int\limits_{\mathcal{L}} \mathsf{j} w_{\rm d}\, da. \tag{5.12}$$

Next, assuming that j is constant over $\mathcal{L}$, we obtain

$$\mathsf{j}(\mathbf{x}_{\rm d}) \approx -\frac{\displaystyle\sum_{\gamma=\alpha,\beta} \int\limits_{\mathcal{B}_\gamma} m_\gamma \mathrm{Grad}\, u\cdot\mathrm{Grad}\, w_{\rm d}\, dv}{\displaystyle\int\limits_{\mathcal{L}} w_{\rm d}\, da} \tag{5.13}$$

for its value at the point $\mathbf{x}_{\rm d}$. We remark that (5.12) may be viewed as a generalization of the superconvergent boundary-flux calculation proposed by Carey et al. (1985), with the

subsequent "lumping" leading to the approximation (5.13). While relatively straightforward, the analogy between Carey's work and domain-integral techniques does not appear to have been drawn before.

We also find it convenient to use the framework developed above to obtain approximate expressions for interfacial normal $\mathbf{n}$ and total curvature K. Specifically, multiplying both sides of $(4.4)_1$ by $w_{\rm d}$ and lumping quantities at the point $\mathbf{x}_{\rm d}$, we obtain

$$\mathbf{n}^e(\mathbf{x}_{\rm d}) \approx \frac{\int\limits_{\mathcal{B}} \dfrac{\operatorname{Grad}\zeta}{|\operatorname{Grad}\zeta|} w_{\rm d}\, dv}{\int\limits_{\mathcal{B}} w_{\rm d}\, dv}; \tag{5.14}$$

similarly, using $(4.4)_2$, we obtain

$$\mathsf{K}^e(\mathbf{x}_{\rm d}) \approx \frac{\int\limits_{\mathcal{B}} \dfrac{\operatorname{Grad}\zeta}{|\operatorname{Grad}\zeta|}\cdot\operatorname{Grad} w_{\rm d}\, dv}{\int\limits_{\mathcal{B}} w_{\rm d}\, dv}. \tag{5.15}$$

To our knowledge, the approximation (5.14) to the interfacial normal is new, but it is merely a simple, weighted average over the support of $w_{\rm d}$. The expression (5.15) for the curvature is a simplified form of that suggested in Barth and Sethian (1998).

6 Discretization with the XFE/LSM

(XFE/LSM)

As in the preceding section, we continue to suppress all dependence upon time.

6.1 Approximation for the motion y

Finite-element computations entail the projection of the solution space $\mathcal{A}_{\rm m}$ and the associated space $\mathcal{V}_0$ of variations onto finite-dimensional subspaces $\mathcal{A}_{\rm m}^h$ and $\mathcal{V}_0^h$. The Galerkin approximation of the variational boundary-value problem stated in Section 5.1 reads: find $\mathbf{y}^h$ in $\mathcal{A}_{\rm m}^h$ such that

$$\sum_{\gamma=\alpha,\beta} \int\limits_{\mathcal{R}_\gamma} \frac{\partial W_\gamma(\mathbf{F}^h)}{\partial \mathbf{F}^h}\cdot\operatorname{Grad}\mathbf{w}^h\, dv = \int\limits_{(\partial\mathcal{R})_{\rm t}} \mathbf{s}\cdot\mathbf{w}^h\, da, \tag{6.1}$$

for all variations $\mathbf{w}^h$ of $\mathbf{y}^h$ belonging to $\mathcal{V}_0^h$.

We use M to denote the total number of elements in the mesh and consider a regular finite-element partition $\mathcal{Q}^h = \cup_{e=1}^M \mathcal{Q}_e$, with $\mathcal{Q}^h = \mathcal{R}$ but with element edges chosen, generally, to be independent of the interface geometry. Letting $P^j(\mathcal{Q}_e)$ denote the space of complete polynomials of order less than or equal to j over element $\mathcal{Q}_e$, we introduce

$$\{\phi_i \in C^0(\mathcal{Q}^h) : \phi_i|\mathcal{Q}_e \in P^j(\mathcal{Q}_e)\}, \tag{6.2}$$

where ϕ_i, $i = 1, 2, \ldots$, are the nodal shape functions. We next consider the set of overlapping subdomains $\{\Omega_i\}$ defining the support of each nodal shape function and an

enrichment function g that possesses desirable approximation properties in a vicinity of the interface. The approximation for the deformation is given by

$$\mathbf{y}^h(\mathbf{x},t) = \underbrace{\sum_{i\in I} \mathbf{c}_i(t)\phi_i(\boldsymbol{\xi}(\mathbf{x}))}_{\text{classical approximation}} + \underbrace{\sum_{j\in J} \mathbf{e}_j(t)\phi_j(\boldsymbol{\xi}(\mathbf{x}))g(\mathbf{x},t)}_{\text{enrichment}}, \tag{6.3}$$

where $\boldsymbol{\xi}$ are the local element coordinates. In the above, I denotes the set of all nodes in the mesh and $J = \{j \in I : \omega_j \cap \mathcal{S} \neq \emptyset\}$ the set of nodes that form a partition of unity for g (Melenk and Babuška, 1996). An example of a two-dimensional mesh with superimposed interface and the subset $J \subset I$ identified is shown in Figure 3.

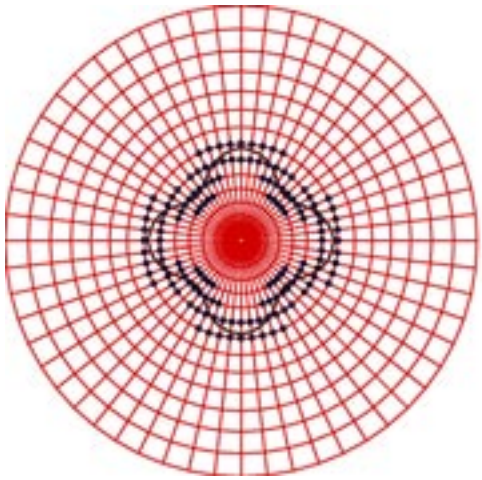

Figure 3: Two-dimensional mesh of four-node quadrilateral elements with an interface $\mathcal{S}$ superimposed. The circled nodes correspond to the subset J that are enriched with the ridge function r to capture gradient discontinuities across the interface.

A number of different enrichment functions have been proposed to capture the discontinuity in the gradient of the motion normal to the interface. Here, we employ the the "ridge" function proposed by Moës et al. (2003):

$$r(\mathbf{x}) = \sum_i |\zeta_i|\phi_i(\boldsymbol{\xi}(\mathbf{x})) - \Big|\sum_i \zeta_i\phi_i(\boldsymbol{\xi}(\mathbf{x}))\Big|, \tag{6.4}$$

where ζ_i is the signed-distance function to the interface evaluated at the vertex of node i. As the discontinuity coincides with the phase interface, the above choice provides a mechanism for the approximation (6.3) to represent the geometry of the interface independent of the element boundaries. Furthermore, as the interface evolves, we update the enrichment function and the set J; no remeshing is performed.

With the preceding definitions, we introduce a set

$$\{\Phi_r\}_{r=1}^N = \{\phi_i\}_{i=1}^{N_I} \cup \{\phi_j\ r\}_{j=1}^{N_J}, \tag{6.5}$$

of linearly independent functions Φ_r; this set forms a basis for $\mathcal{A}_{\mathrm{m}}^h$, where N_I and N_J denote, respectively, the number of elements in the sets I and J and $N = N_I + N_J$. We then represent $\mathcal{A}_{\mathrm{m}}^h$ as

$$\mathcal{A}_{\mathrm{m}}^h = \mathrm{span}\{\Phi_r\}_{r=1}^N. \tag{6.6}$$

We employ a Bubnov–Galerkin approximation and use this same set of functions to construct $\mathcal{V}_{\rm u}^h$.[2]

Substitution of (6.3) into (6.1) results in a nonlinear system of equations in $\{\mathbf{c}_i, \mathbf{e}_j\}$. We employ the standard Newton–Raphson procedure and solve the above with a sequence of linearized problems. These take the form

$$\mathbf{K}_f^{(n)} \Delta \mathbf{d}_f = \mathbf{r}^{(n)}, \tag{6.7}$$

with $\mathbf{K}_f^n$ the tangent stiffness matrix at iteration n, $\mathbf{r}^n$ the residual vector, and $\Delta\mathbf{d}_f$ the vector gathering the incremental degrees of freedom $\Delta\mathbf{c}_i$ and $\Delta\mathbf{e}_j$. After solving the above, the solution is updated in accord with $\mathbf{c}_i^{n+1} = \mathbf{c}_i^n + \Delta\mathbf{c}_i$ and $\mathbf{e}_j^{n+1} = \mathbf{e}_j^n + \Delta\mathbf{e}_j$.

The construction of the tangent stiffness matrix and residual vector requires the accurate integration of terms containing the classical and enriched basis functions over the element subdomains. The standard element-based quadrature routines are modified for those elements wherein the functions are discontinuous. For these "cut" elements in which $\mathcal{S} \cap \mathcal{Q}^e \neq \emptyset$, we first determine the projection

$$\mathcal{S}^e = \left\{ \mathbf{x} \in \mathcal{Q}^e : \sum_i \phi_i(\mathbf{x}) \zeta_i = 0 \right\}, \tag{6.8}$$

of the zero-level set onto the classical basis over the element, where the constants ζ_i correspond to the level-set function evaluated at each of the element's nodes. The complementary subregions $\mathcal{Q}_\beta^e$ and $\mathcal{Q}_\alpha^e$ are then constructed from the intersection of $\mathcal{S}^e$ with $\mathcal{Q}^e$ and each subregion is triangulated for the purposes of integration. It bears emphasis that these "subtriangles" do not lead to the creation of additional degrees of freedom in the global system (6.7). Additional details can be found in Moës et al. (1999) and Dolbow et al. (2000).

6.2 Approximation for the diffusion potential u

The Galerkin approximation to variational boundary-value problem stated in Section 5.2 reads: find u^h in $\mathcal{A}_{\rm p}^h$ and such that

$$\sum_{\gamma=\alpha,\beta} \int\limits_{\mathcal{R}_\gamma} m_\gamma \operatorname{Grad} u^h \cdot \operatorname{Grad} w^h \, dv + \frac{[\![c_\gamma]\!]^2}{\eta} \int\limits_{\mathcal{S}} u^h w^h \, da = - \int\limits_{(\partial\mathcal{R})_{\rm f}} j w^h \, da + \frac{[\![c_\gamma]\!]}{\eta} \int\limits_{\mathcal{S}} (e^h + \sigma \mathsf{K}^h) w^h \, da, \tag{6.9}$$

for all variations w^h of u^h belonging to $\mathcal{V}_{\rm u}^h$.

We note that (6.9) cannot be used in the limit of vanishing reciprocal interfacial mobility. The limiting case can be approximated using small, but finite $\eta > 0$ that essentially plays the role of a penalty parameter enforcing the normal configurational force balance as a Dirichlet constraint on the interface. Alternatives include the introduction of a Lagrange multiplier field, but such a field cannot be selected independently of the approximation to u if optimal rates of convergence are desired (Babuška, 1973).

The approximation for the diffusion potential takes the form

$$u^h(\mathbf{x}, t) = \sum_{i \in I} a_i(t) \phi_i(\boldsymbol{\xi}(\mathbf{x})) + \sum_{j \in J} b_j(t) \phi_j(\boldsymbol{\xi}(\mathbf{x})) r(\mathbf{x}, t), \tag{6.10}$$

[2] The construction of $\mathcal{V}_{\rm u}^h$ employs only those functions Φ_k that vanish on the Dirichlet boundary $(\partial\mathcal{R})_{\rm m}$.

in which $\{\phi_i\}$ is the set of nodal shape functions used in the approximation for the motion. Here, the enrichment allows the approximation u^h to represent the arbitrary gradient discontinuities in the diffusion potential across the interface.

We again adopt a Bubnov–Galerkin approximation and write approximations for the variations w^h in forms similiar to (6.10). Upon substituting the approximations into the discrete weak form (6.9) and invoking the arbitrariness of the variations, we obtain a linear system of equations

$$\mathbf{K}_u \mathbf{d}_u = \mathbf{f}_u, \tag{6.11}$$

where $\mathbf{d}_u$ gathers the degrees of freedom a_i and b_j.

6.3 Discrete versions of domain integrals

Perhaps the most common criticism of domain-integral methods concerns the ambiguity in specifying a discrete local domain $\mathcal{B}^h$ and an approximation w_{d}^h to the weight function. Here, we eliminate both ambiguities.

The discrete version of the domain integral (5.10) begins by considering the set of nodes $D = \{i \in I : \Omega_i \cap \mathbf{x}_{\mathrm{d}} \neq \emptyset\}$ whose support contain the point $\mathbf{x}_{\mathrm{d}}$. The contribution e_k of node $k \in D$ to the mechanical driving traction at a point $\mathbf{x}_{\mathrm{d}}$ on the interface is then given by

$$\mathsf{e}_k(\mathbf{x}_{\mathrm{d}}) = -\frac{\displaystyle\sum_{\gamma=\alpha,\beta} \int\limits_{\mathcal{Q}_\gamma^e \in \Omega_k} \mathbf{n}^h \cdot \mathbf{E}_\gamma(\operatorname{Grad} \mathbf{y}^h)\, \operatorname{Grad} \phi_k \, dv}{\displaystyle\int\limits_{\mathcal{L}^h} \phi_k \, da} - \frac{\displaystyle\sum_{\gamma=\alpha,\beta} \int\limits_{\mathcal{Q}_\gamma^e \in \Omega_k} \operatorname{Grad} \mathbf{n}^h \cdot \mathbf{E}_\gamma(\operatorname{Grad} \mathbf{y}^h) \phi_k \, dv}{\displaystyle\int\limits_{\mathcal{L}^h} \phi_k \, da}. \tag{6.12}$$

Repeating the above calculation for each node in the set D allows us to construct the approximation

$$\mathsf{e}^h(\mathbf{x}_{\mathrm{d}}) = \sum_{i \in D} \mathsf{e}_i(\mathbf{x}_{\mathrm{d}}) \phi_i(\boldsymbol{\xi}(\mathbf{x}_{\mathrm{d}})). \tag{6.13}$$

This approach removes the need to specify a local domain size multiplier and search for a set of nodes within the corresponding radius at each point of interest on the interface. In effect, only those nodes with support containing the point $\mathbf{x}_{\mathrm{d}}$ contribute to the approximation to e.

The above expression involves an approximation $\mathbf{n}^h$ to the extended normal $\mathbf{n}^e$ obtained from the level-set function ζ. Consistent with the above, we use

$$\mathbf{n}^h(\mathbf{x}_{\mathrm{d}}) = \sum_{i \in D} \mathbf{n}_i^e(\mathbf{x}_{\mathrm{d}}) \phi_i(\boldsymbol{\xi}(\mathbf{x}_{\mathrm{d}})), \tag{6.14}$$

where the coefficients $\mathbf{n}_i^e(\mathbf{x}_{\mathrm{d}})$ denote lumped approximations to the extended normal. For the approximation K^h to the curvature appearing in the Galerkin approximation (6.9) to

u, we likewise take

$$\mathsf{K}^h(\mathbf{x}_\mathrm{d}) = \sum_{i\in D} \mathsf{K}_i^e \mathbf{x}_\mathrm{d} \phi_i(\boldsymbol{\xi}(\mathbf{x}_\mathrm{d})), \tag{6.15}$$

with the constants $\mathsf{K}_i^e(\mathbf{x}_\mathrm{d})$ denoting lumped approximations to the extended curvatures at the nodes. The coefficients $\mathbf{n}_i^e(\mathbf{x}_\mathrm{d})$ and $\mathsf{K}_i^e(\mathbf{x}_\mathrm{d})$ are both determined using the approximation ζ^h to the level-set function ζ, as described in the next section.

The discrete form of (5.12) is given by

$$\mathsf{j}^h(\mathbf{x}_\mathrm{d}) = \sum_{i\in D} \mathsf{j}_i(\mathbf{x}_\mathrm{d}) \phi_i(\boldsymbol{\xi}(\mathbf{x}_\mathrm{d})), \tag{6.16}$$

with

$$\mathsf{j}_k(\mathbf{x}_\mathrm{d}) = -\frac{\displaystyle\sum_{\gamma=\alpha,\beta} \sum_e \int\limits_{\mathcal{Q}_\gamma^e \in \Omega_k} m_\gamma \mathrm{Grad}\, u^h \cdot \mathrm{Grad}\, \phi_k \, dv}{\displaystyle\int\limits_{\mathcal{L}^h} \phi_k \, da}. \tag{6.17}$$

In the special case when the interface is coincident with a set of element edges, it can be shown that the above reduces to the superconvergent flux calculation proposed by Carey et al. (1985).

7 Level-set algorithm and coupling with bulk fields

We consider the finite-element triangulation $\mathcal{T}^h = \cup_{e=1}^M \mathcal{T}_e$, with $\mathcal{T}^h = \mathcal{R}$, and with vertex set chosen to be identical to that of $\mathcal{Q}^h$.[3] The function ζ is approximated using the piecewise-linear finite-element subspace

$$\mathcal{Z}^h = \{N_i \in C^0(\mathcal{T}^h) : N_i|\mathcal{T}_e \in P^1(\mathcal{T}_e)\}, \tag{7.1}$$

where N_i denotes the shape function for node i.

With the above definitions, we write

$$\zeta^h(\mathbf{x}) = \sum_i \zeta_i N_i(\mathbf{x}), \tag{7.2}$$

for the approximation to the function ζ.

Substitution of (7.1) and (7.2) directly into (4.4) leads to expressions for $\mathbf{n}^e$ and K^e that are constant or vanish over each element $\mathcal{T}_e$. The extended normal and total curvature are much more accurately approximated using discrete versions of (5.14) and (5.15), respectively. Thus, about each vertex in the vicinity of the interface we calculate

$$\mathbf{n}_i^e = \frac{\displaystyle\int\limits_{\mathcal{T}_e \in \Omega_i} \frac{\mathrm{Grad}\, \zeta^h}{|\mathrm{Grad}\, \zeta^h|} N_i \, dv}{\displaystyle\int\limits_{\mathcal{T}_e \in \Omega_i} N_i \, dv} \tag{7.3}$$

[3] Both meshes are constructed using the code `gmsh` (Remacle and Geuzaine, 1998).

and

$$\mathsf{K}_i^e = \frac{\displaystyle\int_{\mathcal{T}_e \in \Omega_i} \frac{\operatorname{Grad}\zeta^h}{|\operatorname{Grad}\zeta^h|}\cdot\operatorname{Grad}N_i\,dv}{\displaystyle\int_{\mathcal{T}_e \in \Omega_i} N_i\,dv} \tag{7.4}$$

for use in the expansions (6.14) and (6.15).

For the level-set equation (4.2), we use the positive-coefficient scheme proposed by Barth and Sethian (1998). The basic procedure is as follows. We assume that the nodal coefficients ζ_i are known at some time t^n; we denote these by ζ_i^n. Further, we assume that the extension velocity v^e is also known. The goal is to determine the coefficients ζ_i^{n+1} describing the evolution of the level-set function to time t^{n+1}, and, accordingly, the zero-level set.

We first initialize a set of temporary coefficients ζ_i^* and w_i at each node to zero. We then loop over each element and compute

$$\operatorname{Grad}\zeta^h = \sum_{i=1}^{3}\zeta_i^n\operatorname{Grad}N_i, \qquad \bar{v}^e = \int_{\mathcal{T}_e} v^e\,dv. \tag{7.5}$$

Since the gradient of each shape function is constant over the element, so too is $\operatorname{Grad}\zeta^h$, and $(7.5)_1$ can be calculated at any point on $\mathcal{T}_e$. On each element, we also compute

$$K_i = \bar{v}^e\frac{\operatorname{Grad}\zeta^h}{|\operatorname{Grad}\zeta^h|}\cdot\operatorname{Grad}N_i, \qquad i = 1\ldots 3, \tag{7.6}$$

and

$$\delta\zeta^h = \sum_{i=1}^{3}K_i\zeta_i^n, \qquad \tilde{\alpha}_i = \frac{H(\delta\zeta_i/\delta\zeta^h)}{\sum_{j=1}^{3}H(\delta\zeta_j/\delta\zeta^h)} \quad i = 1\ldots 3, \tag{7.7}$$

with

$$\delta\zeta_i = H(K_i)\left(\sum_{l=1}^{3}H(K_l)\right)^{-1}\sum_{j=1}^{3}H(-K_j)(\zeta_i-\zeta_j) \tag{7.8}$$

and H defined so that $H(f) = \max\{0, f\}$. Having determined the above coefficients on $\mathcal{T}_e$, we then update the nodal coefficients ζ_i^* and w_i at each node of the element by

$$\zeta_i^* = \zeta_i^* + \tilde{\alpha}_i, \qquad w_i = w_i + \tilde{\alpha}_i\ \operatorname{meas}(\mathcal{T}_e). \tag{7.9}$$

With the contributions to w_i and ζ_i^* of each element in the mesh thus being assembled, the nodal coefficients ζ_i^{n+1} are integrated in time by the first-order scheme

$$\zeta_i^{n+1} = \zeta_i^n - \Delta t\frac{\zeta_i^*}{w_i}. \tag{7.10}$$

The above strategy requires the specification of the extension velocity v^e over the entire domain. The normal velocity v is first determined on each subsurface $\mathcal{S}^e$ using the domain integral approximation (6.16) to the jump in normal component of solute flux and the interfacial solute balance $(3.11)_2$. We then loop over the elements in the triangulation $\mathcal{Z}^h$ and determine the closest point between each element center and the

discrete representation of the interface through the set of subsurfaces $\{\mathcal{S}^e\}$. We take the extension velocity to be constant over each element $\mathcal{T}_e$, and assign its value to be that of the closest point projection. A similar strategy was proposed by Garikipati and Rao (2001).

In closing this section, we remark that our strategy does give rise to a small discrepancy between the representation of the zero-level set on the subspaces $\mathcal{Z}^h$ and $\mathcal{Q}^h$ used for the level-set algorithm and the representation of the bulk fields, respectively. Although the meshes share the same set of vertices, fields represented on $\mathcal{Q}^h$ are bilinear over each element whereas those represented on $\mathcal{Z}^h$ are only linear. We could have represented the bulk fields using the triangulation $\mathcal{Z}^h$, but we find the enriched bilinear quadrilaterals yield considerably more accurate results. Further, while the use of least-squares stabilized finite-element algorithms do exist for discretizing (4.2) over $\mathcal{Q}^h$ (as well as over $\mathcal{Z}^h$), such algorithms typically add some form of non-linear artificial viscosity requiring user-specified parameters. By contrast, no free parameters are present in (7.5)-(7.10).

8 Staggered solution strategy

We now describe the solution strategy for the full system. Assuming that all fields and the geometry of the interface $\mathcal{S}$ are known at some time t^n, the first step is to advect the level-set function using the algorithm (7.5)–(7.10), and, thereby, to obtain the position of the interface at time t^{n+1}. The nonlinear system (6.7) is then solved and the mechanical fields are post-processed using the domain integral approximation (6.13) to obtain the mechanical contribution e^h to the normal configurational force balance. The approximation ζ^h to the level-set field is similarly post-processed using (6.15) and (7.4) to obtain the smoothed approximation K^h to the total curvature of the interface. Finally, the approximation for the diffusion potential is obtained by solving (6.11), completing the determination of all bulk fields at time t^{n+1}. The solution of (6.11) is then post-processed to obtain the normal interfacial velocity through $(3.11)_2$ and the domain integral approximation (6.16). The above process is then repeated. This strategy is exact and does not require iteration within a time step.

The feasibility of the above solution strategy rests on the constitutive specializations described in Section 3, which lead to equations in which the coupling between the deformation and diffusion potential is solely through the interfacial conditions. In the more general equations (2.50) and (2.51), the strong coupling of the bulk fields would require an alternative strategy.

9 Numerical investigations

In the sections that follow, we describe studies designed to show how particular material parameters in the model influence the numerical predictions. The normalized baseline quantities for our studies are provided in Table 1. We investigate two-dimensional problems and assume that plane-strain conditions hold.

9.1 Benchmark studies

We now describe benchmark studies that examine the accuracy of the enriched approximations $\mathbf{y}^h$ and u^h to the motion and diffusion potential. We also present results that substantiate the use of the domain integral representations of interfacial quantities. Whenever possible, we compare our results to analytical solutions as well as those obtained with classical, unenriched finite-element bases.

Property	Normalization	Collapsed phase (β)	Swelled phase (α)
c_γ	c_γ	0.9	0.1
m_γ	$\dfrac{m_\gamma\, T\Theta}{Z^2(c_\beta - c_\alpha)}$	1.0	2.0
σ	$\dfrac{\sigma}{Z(c_\beta - c_\alpha)\Theta}$	0.01	0.01
η	$\dfrac{\eta Z}{T(c_\beta - c_\alpha)\Theta}$	0.01	0.01
μ_γ	$\dfrac{\mu_\gamma}{(c_\beta - c_\alpha)\Theta}$	0.01	0.005
λ_γ	$\dfrac{\lambda_\gamma}{(c_\beta - c_\alpha)\Theta}$	0.05	0.01
J_γ	J_γ	1.0	10.0
w_γ	$\dfrac{w_\gamma}{(c_\beta - c_\alpha)\Theta}$	0.0	0.02

Table 1: Baseline material properties and parameters used in the parametric studies. Normalized quantities are provided based on a gel with characteristic length Z, characteristic swelling time T, and characteristic value Θ of the diffusion potential.

We assess accuracy through suitably-defined error norms. For the approximation f^h to a bulk field f, we employ the relative error norms

$$\mathcal{E}_L(f, f^h) \equiv \sqrt{\frac{\displaystyle\sum_{\gamma=\alpha,\beta} \int\limits_{\mathcal{R}_\gamma} (f - f^h)^2 \, dv}{\displaystyle\sum_{\gamma=\alpha,\beta} \int\limits_{\mathcal{R}_\gamma} f^2 \, dv}}, \tag{9.1}$$

and

$$\mathcal{E}_H(f, f^h) \equiv \sqrt{\frac{\displaystyle\sum_{\gamma=\alpha,\beta} \int\limits_{\mathcal{R}_\gamma} |\mathrm{Grad}\,(f - f^h)|^2 \, dv}{\displaystyle\sum_{\gamma=\alpha,\beta} \int\limits_{\mathcal{R}_\gamma} |\mathrm{Grad}\, f|^2 \, dv}}. \tag{9.2}$$

Similarly, to assess the accuracy of the approximation f^h to an interfacial field f, we use the relative error norm

$$\mathcal{E}_{\mathcal{S}}(\mathsf{f}, \mathsf{f}^h) \equiv \sqrt{\frac{\displaystyle\int\limits_{\mathcal{S}} \left(\mathsf{f} - \mathsf{f}^h\right)^2 \, da}{\displaystyle\int\limits_{\mathcal{S}} \mathsf{f}^2 \, da}}. \tag{9.3}$$

9.1.1 Static two-phase states

We begin by considering a cylindrical gel specimen, with radius R, the lateral surface of which is traction free and in contact in a reservoir of uniform diffusion potential U. For the artificial problem wherein the position of the interface $\mathcal{S}$ is held fixed, we seek approximations to $\mathbf{y}$ and u.

We first examine the case of an interface geometry that is self-similar to the specimen, i.e.

$$\mathcal{S} = \{\mathbf{x} : |\mathbf{x}| = r_{\mathsf{s}}, r_{\mathsf{s}} < R\}, \tag{9.4}$$

for which it can be shown that the diffusion potential varies only with radial position r as

$$u(r) = U + \frac{[\![c_\gamma]\!]\,(r_{\mathsf{s}} U [\![c_\gamma]\!] - r_{\mathsf{s}}\mathsf{e} - \sigma)}{\eta m_\alpha + [\![c_\gamma]\!]^2 r_{\mathsf{s}} \log \frac{R}{r_{\mathsf{s}}}} \begin{cases} \log \dfrac{r_{\mathsf{s}}}{R}, & r \le r_{\mathsf{s}}, \\ \log \dfrac{r}{R}, & r_{\mathsf{s}} \le r \le R, \end{cases} \tag{9.5}$$

with $\mathsf{e} = \mathbf{n} \cdot [\![\mathbf{E}_\gamma(\mathbf{F})]\!]\mathbf{n}$ the mechanical driving traction. The explicit expression (9.5) for u satisfies the bulk solute balance $(3.10)_2$, the requirement (2.31) of local chemical equilibrium, the normal configurational force balance $(3.11)_3$, and the boundary condition $(2.54)_1$.

We consider a gel specimen with the material properties listed in Table 1, and choose $r_{\mathsf{s}}/R = \frac{1}{4}$, with $R/Z = 2.0$. The influence of the motion $\mathbf{y}$ on the above solution is solely through the mechanical driving traction e. Since an analytical expression for the motion $\mathbf{y}$ is not available for the above case, we first obtain a converged numerical approximation $\mathbf{y}^h$ by solving (6.7) using a sequence of meshes of four-node quadrilateral elements. The meshes are constructed by placing mesh lines along the radial and circumferential directions, as shown in Figure 4a. Figure 4a also plots the normalized quantity $\mathsf{e}/[\![c_\gamma]\!]\Theta$ obtained using the domain integral approximation (6.13) with a sequence of increasingly refined meshes. The results converge to a normalized value of approximately -0.228. We observe that even with the initial, coarse mesh, the results obtained with the domain integral method are within 1% of the converged result.

Figure 4b shows the results of a similar study, with the mechanical driving traction obtained by directly evaluating $\mathsf{e}^h = \mathbf{n} \cdot [\![\mathbf{E}_\gamma(\mathrm{Grad}\,\mathbf{y}^h)]\!]\mathbf{n}$ on the interface. Although these results do converge to the same result shown in Figure 4a, the coarse mesh results are far less accurate. They also exhibit much larger oscillations than those shown in Figure 4a. Clearly, the domain integral approximation (6.13) to the mechanical driving traction is more robust than a direct evaluation.

In the studies described below, we solve the matrix system of equations (6.11) using the converged numerical approximation to e. We take the square region $\mathcal{R}^h = [0, R/2] \times [0, R/2]$ as the computational domain and impose the Lagrange interpolant to the solution (9.5) as a Dirichlet boundary condition along the upper and right surfaces, and impose symmetry conditions along the lower and left surfaces (Figure 5). This geometry facilitates the construction of uniform Cartesian meshes that can be systematically refined. We report results for a sequence of partitions using four-node quadrilateral elements. Importantly, for these studies, the interface geometry is not coincident with element edges.

Shown in Figure 6 are the error norms $\mathcal{E}_L(u, u^h)$ and $\mathcal{E}_H(u, u^h)$ (cf. (9.1) and (9.2)) computed using both the classical and the enriched approximations for u as a functions of the nodal spacing h. With enrichment, we observe quadratic convergence in $\mathcal{E}_L$ and linear convergence in $\mathcal{E}_H$. Those rates would be expected of a classical approximation to

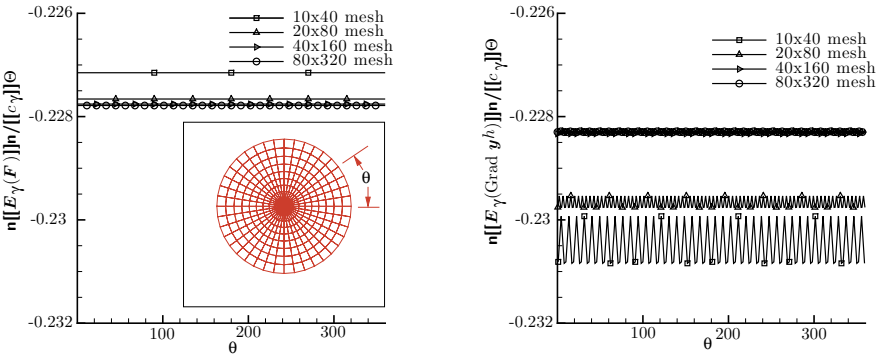

(a) Domain-integral results.

(b) Direct-evaluation results.

Figure 4: Normalized mechanical driving traction as a function of the angle θ for a sequence of meshes obtained using a) the domain-integral method and b) direct evaluation. Each mesh has a uniform number of partitions in the radial and circumferential directions, with a 10×40 mesh shown in the insert of a).

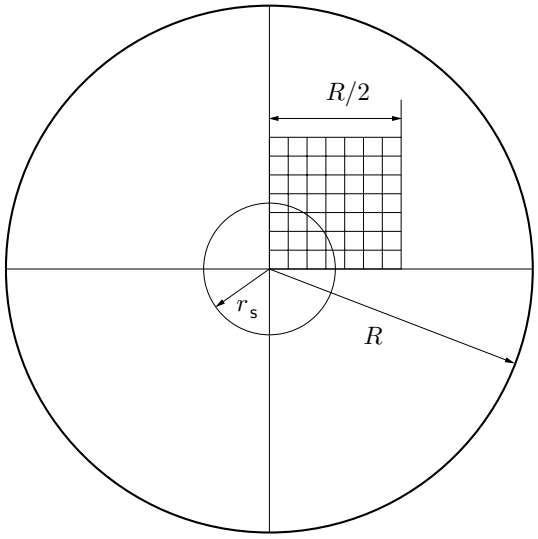

Figure 5: A square computational domain isolated from one quarter of the cylindrical gel specimen and uniformly partitioned with four-node quadrilateral elements. The radius of the phase interface is $r_s = R/4$.

u using a sequence of fitted meshes. As shown in Figure 6, using these same Cartesian meshes without enriching the approximation to u leads to a marked decrease in the rates of convergence and accuracy.

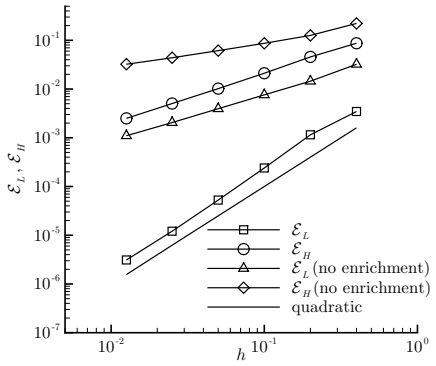

Figure 6: Relative error norms $\mathcal{E}_L(u, u^h)$ and $\mathcal{E}_H(u, u^h)$ as a function of characteristic mesh size h obtained for a static two-phase state problem on a cylindrical specimen with self-similar interface.

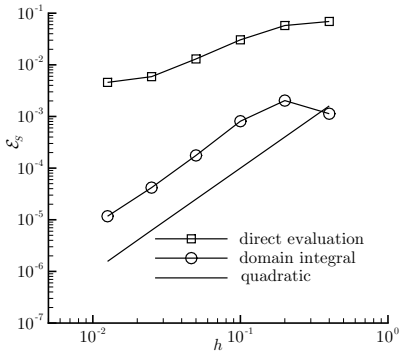

Figure 7: Relative error norm $\mathcal{E}_S(\mathsf{j}, \mathsf{j}^h)$ of the jump in the normal component of solute flux of a static two-phase state problem on a cylindrical specimen with self-similar interface.

We next examine the accuracy of various approximations to the jump $\mathsf{j} = [\![\mathbf{j}]\!]\cdot\mathbf{n}$ in the normal component of solute flux at the interface. Convergence plots in the normalized interfacial error norm $\mathcal{E}_S(\mathsf{j}, \mathsf{j}^h)$ (cf. (9.3)) for the same specimen and interface geometry are shown in Figure 7. The error in j obtained with the domain integral method converges at a nearly quadratic rate. Such a rate is consistent with that obtained using the superconvergent flux post-processing technique discussed in Pehlivanov et al. (1992).[4] For comparison, we also examine the accuracy of approximating j through direct evaluation of the gradient $\mathrm{Grad}\, u^h$ on the interface, i.e. through

$$\mathsf{j}^h = [\![m_\gamma \mathrm{Grad}\, u^h]\!]\cdot\mathbf{n}. \tag{9.6}$$

The results shown in Figure 7 indicate that this approximation is not only much less accurate than that obtained using the domain integral method but also converges at only a linear rate. Similar results were reported by Ji and Dolbow (2004).

We next examine the accuracy of the domain-integral approximations (6.14) and (6.15) to the interfacial normal and curvature. The results shown in Figure 8 indicate that those approximations both converge quadratically with the mesh spacing h. By contrast, the direct evaluation of the normal obtained through $(4.4)_1$ by post-processing ζ^h on the interface is far less accurate and exhibits only linear convergence. While not shown in the Figure, the direct evaluation of the curvature obtained through $(4.4)_2$ by post-processing ζ^h does not converge.

9.1.2 Transient benchmark

We again consider a cylindrical specimen, with a concentric interface of initial radius $r_{\mathsf{s}}/R = 0.9$, immersed in a reservoir with uniform diffusion potential U. Computing the

[4] The results presented in this study are for simply connected, closed interfaces, possessing null intersection with the boundary. Increased errors at boundaries decrease the theoretical rate convergence for this technique by one-half an order in h.

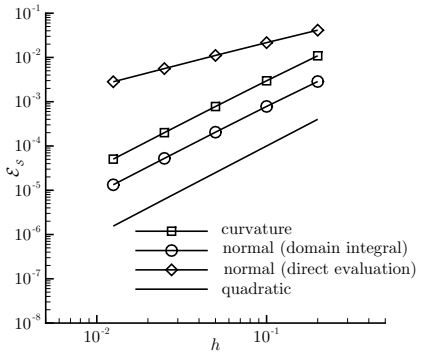

Figure 8: Relative error norms $\mathcal{E}_{\mathcal{S}}(\mathbf{n}, \mathbf{n}^h)$ and $\mathcal{E}_{\mathcal{S}}(\mathsf{K}, \mathsf{K}^h)$ as a function of characteristic mesh size h obtained for a static two-phase state problem on a cylindrical specimen with self-similar interface.

interfacial limits of $\operatorname{Grad} u$ from (9.5) and using those limits in $(3.11)_2$, we obtain

$$\mathsf{v}(r_{\mathsf{s}}) = -\frac{m_\alpha \left(r_{\mathsf{s}} U [\![c_\gamma]\!] - r_{\mathsf{s}} \mathsf{e} - \sigma\right)}{r_{\mathsf{s}} \left(\eta m_\alpha + [\![c_\gamma]\!]^2 r_{\mathsf{s}} \log \frac{R}{r_{\mathsf{s}}}\right)}. \tag{9.7}$$

An analytical expression for the mechanical driving traction e is not available. We therefore set $\mathsf{e} = 0$ in (9.7) and use the resulting expression as a transient benchmark.

We follow the staggered solution strategy described in Section 8, but with $\mathsf{e} = 0$. We also set $U/\Theta = -1.0$, in which case the radius of the interface decreases with time. Figures 9a and and 9b compare the XFE/LSM results for the average radius and velocity of the front to those obtained by integrating (9.7). We find good correlation between the numerical and theoretical results for both the radius and velocity, even on relatively coarse meshes. The results shown in Figure 9a also exhibit behavior qualitatively similar to that reported by Dolbow et al. (2004) for the swelling of spherical specimens and by Barriere and Leibler (2003).

9.2 Kinetic response

We now solve the fully coupled system of equations (3.10)–(3.11) using the staggered strategy described in Section 8. We assume a cylindrical geometry for the specimen in the reference configuration and impose a constant diffusion potential U on the lateral surface of the specimen. We examine how the interface evolves for a specified initial geometry and material parameters.

9.2.1 Self-similar interface evolution

We again consider a gel specimen, with cylindrical reference shape, immersed in a solvent with uniform diffusion potential $U/\Theta = -1.0$. We take the interface to be initially located at $r_{\mathsf{s}}/R = 0.9$ and follow the staggered solution strategy described in Section 8. Using the material properties provided in Table 1, we find the mechanical driving traction e is negative throughout the simulation. In comparison to the studies described in Section 9.1.2, in which the contribution of e to the configurational force balance was

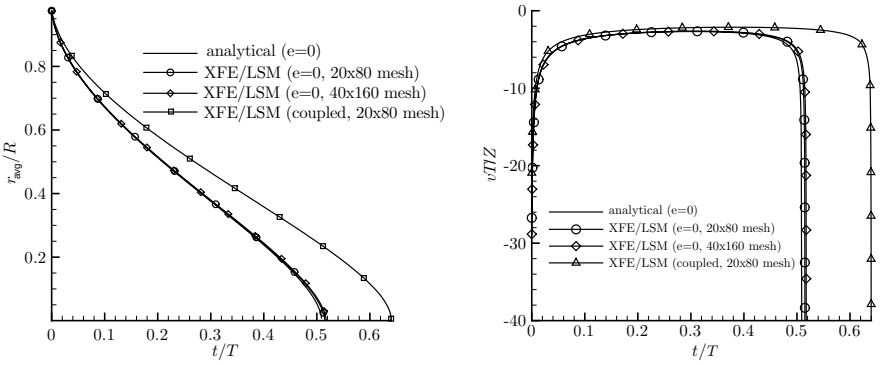

(a) Average interfacial radius.

(b) Average interfacial velocity.

Figure 9: Normalized a) average interfacial radius and b) average interfacial velocity for an evolving cylindrical interface. Results are shown with the mechanical driving traction e artificially neglected and included in the normal configurational force balance.

neglected, we find a decrease in the normal velocity. This is consistent with the analytical solution (9.7) for the interfacial velocity when, as assumed in the problem under consideration, $U < 0$. A comparison of the average interfacial radius and velocity versus time, as depicted in Figures 9a and 9b, clarifies the influence of the mechanical driving traction during swelling.

Figure 10 depicts, for the interface position $r_{\mathsf{s}}/R = 0.5$ the normalized radial and circumferential components of the Cauchy stress tensor $\mathbf{T} = \mathbf{S}\mathbf{F}^{\top}/\det\mathbf{F}$, along a radial line in the deformed configuration. The location of the interface is clear from both the jump in the hoop stress and the kink in the radial stress at $|\mathbf{y}|/R \approx 0.5$. These results are consistent with those reported in Dolbow et al. (2004) in the sense that the mismatch in material moduli across the interface gives rise to a tensile hoop stress in the collapsed phase and a compressive hoop stress in the swelled phase.

Figure 11 shows the radial component of the instantaneous velocity field when the interface is located at $r_{\mathsf{s}}/R = 0.5$. These results are obtained by post-processing the deformation $\mathbf{y}^h$ at two subsequent time steps and dividing the difference by the step-size Δt. We note that the collapsed core remains almost stationary; most of the motion is confined to the swelled phase. These results bear a strong resemblance to the experimental measurements of deformation rates in cylindrical microgel specimens reported by Olsen et al. (2000).

9.2.2 Perturbed interface evolution

We next investigate the conditions for unstable growth of the interface by adding small perturbations to its initial geometry. Specifically, choosing a rectangular cartesian coordinate system with origin at the center of the specimen and denoting by θ the counterclockwise angle from the horizontal axis, we take the initial interface geometry to be

$$\mathcal{S} = \{\mathbf{x} : |\mathbf{x}| = r_p(\theta)\}, \tag{9.8}$$

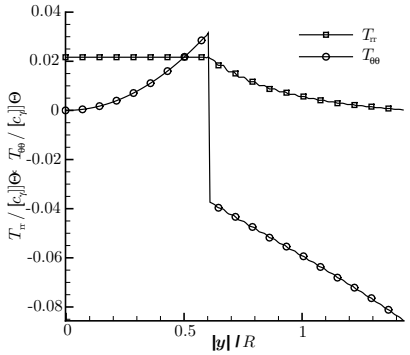

Figure 10: Normalized radial and circumferential components of the Cauchy stress tensor along a radial line in the deformed configuration.

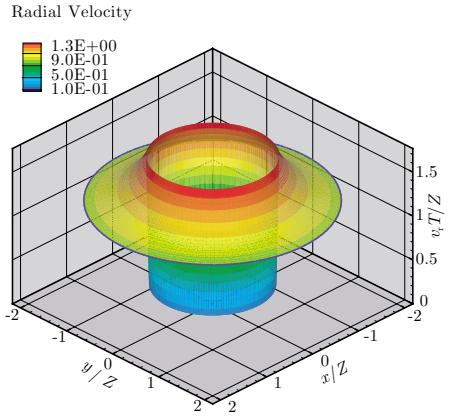

Figure 11: Instantaneous radial component of the normalized velocity field in the cylindrical specimen.

with

$$r_p(\theta) = r_s + p\cos(n\theta). \tag{9.9}$$

We set $r_s/Z = 0.4$, $p/Z = 0.02$ and $n = 5$, corresponding to a 5%, 5-fold symmetric perturbation. We set the value of the diffusion potential at the boundary of the specimen to be $U/\Theta = 2.0$. As a result, the interface evolves toward the free surface of the specimen while the swelled phase transitions to the collapsed phase. We find that sufficiently converged results are obtained using a 30×120 mesh. All results reported in this section are for that level of refinement.

We first investigate the influence of the interfacial free-energy density σ on the evolution of the interface. The results are presented in Figure 12 for various magnitudes of the dimensionless interfacial free-energy density $\sigma/Z[\![c]\!]\Theta$ with all other dimensionless material parameters fixed at those given in Table 1. In each case, the geometry of the interface in the reference configuration is shown at equally-spaced time intervals. For a relatively small value of $\sigma/Z[\![c]\!]\Theta = 0.001$, the perturbation of the interface is observed to evolve into long and slender "fingers." Larger values of the interfacial free-energy density both decrease the average velocity of the interface and stabilize the perturbation. For values of $\sigma/Z[\![c]\!]\Theta$ above 0.1, perturbations of the interface decay with time.

To characterize the growth/decay of the perturbation, at each time step t^n we calculate the deviation

$$d = \sqrt{\frac{\displaystyle\int_{\mathcal{S}} (r - r_{\text{avg}})^2 \, da}{\displaystyle\int_{\mathcal{S}} r_{\text{avg}}^2 \, da}}, \tag{9.10}$$

from the average radius r_{avg}. The deviation as a function of normalized time is plotted in Figure 13. For values of $\sigma/Z[\![c]\!]\Theta$ between 0.04 and 0.1, the perturbation decays initially but then grows as the interface approaches the free surface of the specimen. Figure 14 shows the deformed mesh at the beginning and towards the end of the simulation for the

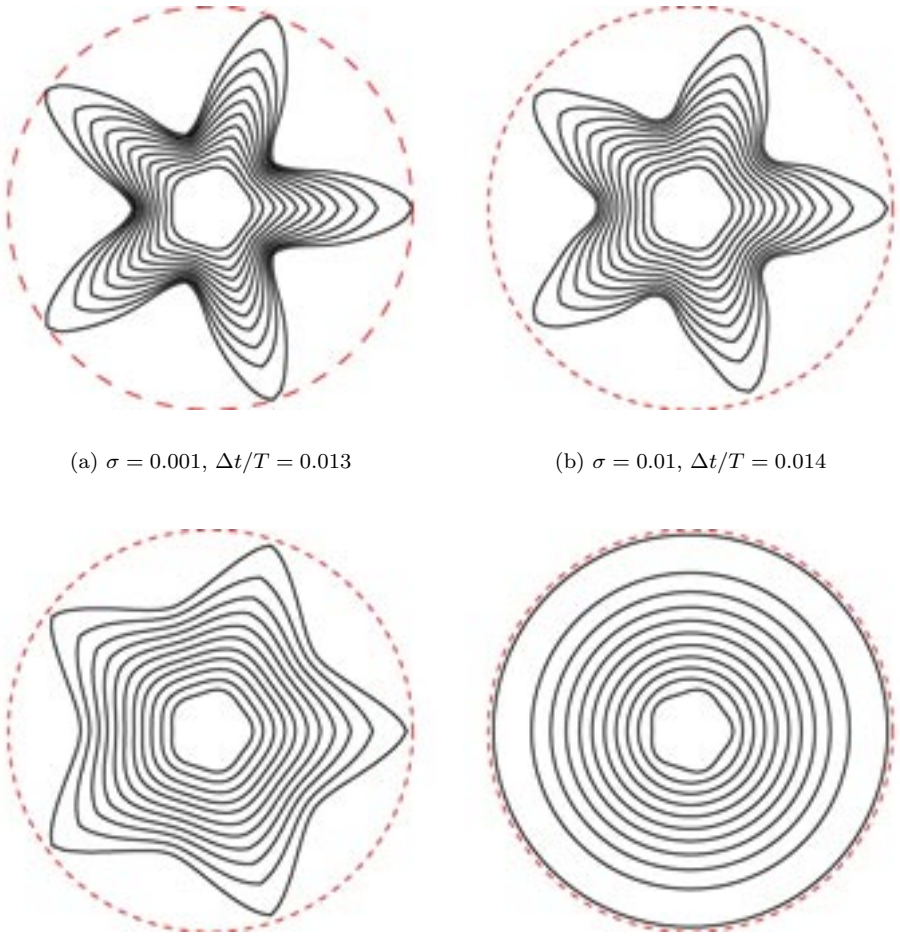

(a) $\sigma = 0.001$, $\Delta t/T = 0.013$

(b) $\sigma = 0.01$, $\Delta t/T = 0.014$

(c) $\sigma = 0.02$, $\Delta t/T = 0.017$

(d) $\sigma = 0.1$, $\Delta t/T = 0.02$

Figure 12: Interface geometries in the reference configuration for various magnitudes of the normalized interfacial free-energy density σ. The dashed lines denote the surface of the gel specimen in the reference configuration.

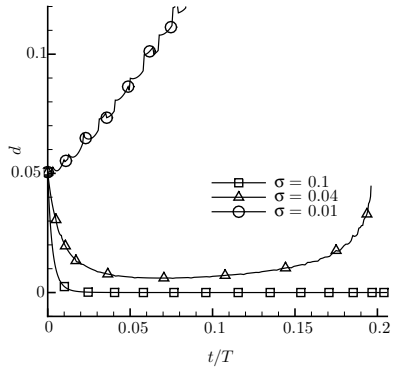

Figure 13: Percent deviation d from the average radius as a function of normalized time for different values of the normalized interfacial free-energy density $\sigma/Z[\![c]\!]\Theta$.

case when $\sigma/Z[\![c]\!]\Theta = 0.04$. Initially, the influence of the perturbed interface geometry is not visible on the surface of the specimen. Towards the end of the simulation, when $t/T = 0.18$, the magnitude of the perturbation is approximately 2%. Nevertheless, the influence of this small perturbation on the motion $\mathbf{y}$ is clearly exhibited by the pattern that forms on the surface of the specimen as shown in Figure 14.

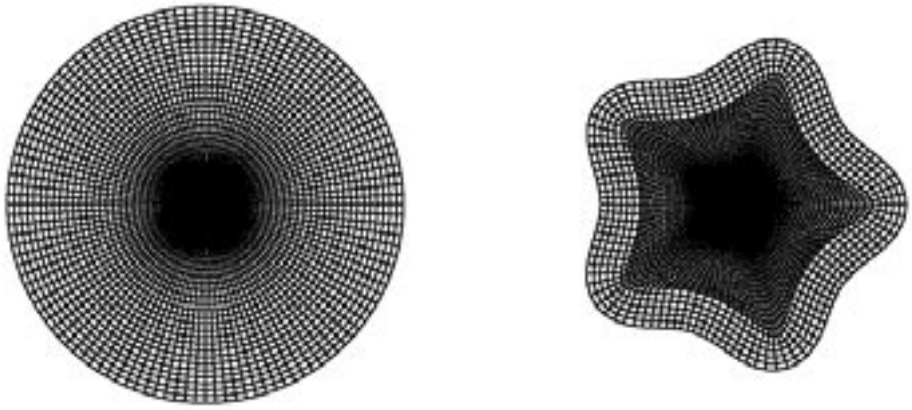

Figure 14: Deformed meshes at $t/T = 0.0$ (left) and at $t/T = 0.18$ (right) corresponding to the evolution of an initially perturbed interface with normalized $\sigma = 0.04$.

We performed additional studies to examine the role of the reciprocal interfacial mobility η. Our results indicate that increasing $\eta Z/T[\![c]\!]\Theta$ results in a decrease of the interfacial velocity. This is consistent with the dissipative role of η in the theory. Importantly, however, for values of $\sigma/Z[\![c]\!]\Theta$ below 0.05, it is not possible to stabilize the interface by increasing $\eta Z/T[\![c]\!]\Theta$. The interface geometry in the reference configuration at equally spaced time steps is shown for select η in Figure 15.

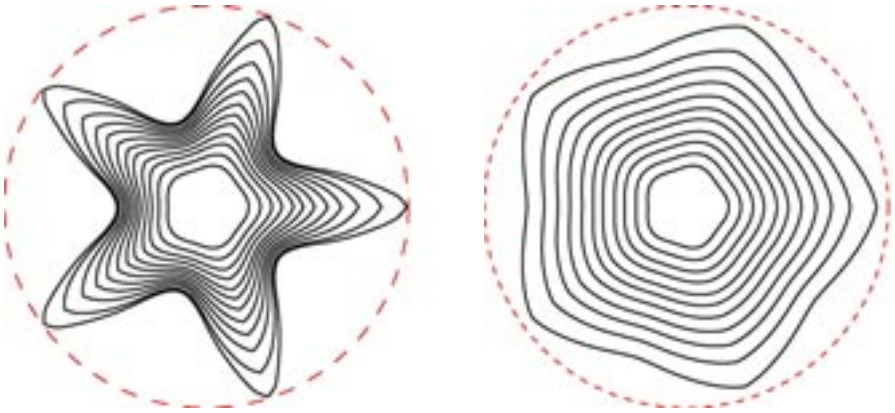

(a) $\eta = 0.001$, $\Delta t/T = 0.012$ (b) $\eta = 0.1$, $\Delta t/T = 0.024$

Figure 15: Interface geometry at uniform increments of $\Delta t/T$ for select values of the reciprocal interfacial mobility η. The dashed lines denote the boundary of the gel specimen.

Finally, we were able to use our strategy to observe bulk phase separation. Figure 16 shows the evolution of the interface at equally spaced time intervals obtained using $\sigma/Z[\![c]\!]\Theta = 0.01$ and $\eta Z/T[\![c]\!]\Theta = 0.001$. Once the interface reaches the boundary of the specimen, the topology of the front changes from a simply-connected surface to five disjoint surfaces. A short time after the topology change, the interface accelerates and small, isolated pockets of the swelled phase can be observed. Those pockets eventually disappear with the completion of the phase transition. We note that a rather dramatic deformation occurs when the interface first breaks through the surface of the specimen and the topology of the phase interface changes. In many of the cases we examined, this gives rise (briefly) to a breakdown—at the surface of the specimen—in the invertibility of the motion $\mathbf{y}$. Such noninvertibility is clearly non-physical. While imposing contact conditions on the motion at the surface of the specimen would preclude this, the results shown in Figure 16 were obtained without such a constraint.

10 Summary and concluding remarks

In this paper, we provided a generalized form of our sharp-interface theory for chemically-induced phase transitions in stimulus-responsive hydrogels. Motivated by experimental observations, we specialized the theory to situations in which the time-scale associated with the motion of the interface is slow with respect to bulk solute diffusion.

Building upon the previous works of Dolbow et al. (2004) and Ji and Dolbow (2004), we developed a numerical strategy to obtain approximate solutions to the nonlinear evolution equations. This entailed first representing the interface as a zero-level set and recasting the evolution equations into equivalent variational forms. Domain-integral representations of the mechanical driving traction, interfacial normal, interfacial curvature, and jump in solute flux were also provided. Enriched finite-element approximations to the diffusion potential and motion were then described. A ridge function was used for enrichment in both cases, allowing the fields to exhibit the correct slope discontinuities across the phase interface. Discrete forms of the domain-integral representations were developed without the use of arbitrary domain-size multipliers advocated elsewhere. We described

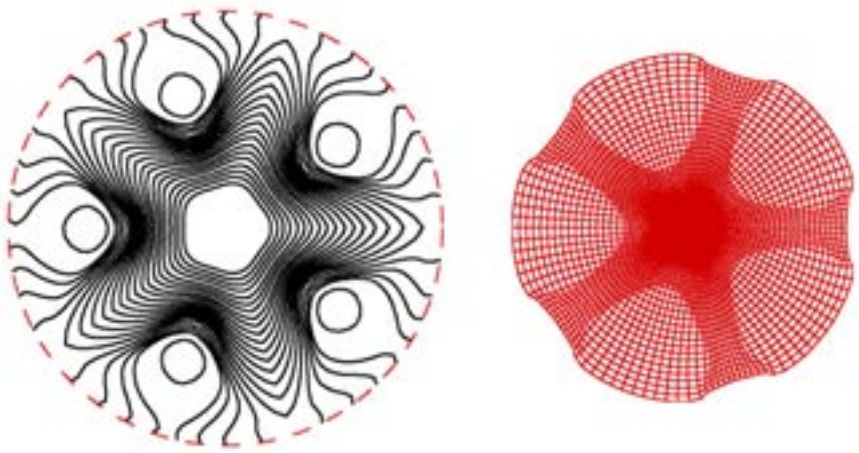

Figure 16: Interface geometry in the reference configuration at equally spaced time intervals $\Delta t/T = 0.008$ (left) and the deformed mesh at $t/\Delta t = 18$ (right) corresponding to the evolution of an initially perturbed interface with $\sigma/Z[\![c]\!]\Theta = 0.01$ and $\eta Z/T[\![c]\!]\Theta = 0.001$.

our procedure for coupling these finite-element and domain-integral approximations to a finite-difference, positive-coefficient scheme for advecting the discrete representation of the interface.

The results from several benchmark studies were presented to demonstrate robustness of the numerical methodologies. In comparison to the existing alternatives, we showed that the combination of enrichment and post-processing with domain integrals provided a marked improvement in accuracy and rates of convergence in both bulk and interfacial error norms. We then presented results from our examinations of swelling kinetics in cylindrical specimens. For stable, self-similar interface evolution, we obtained results for the deformation rate that compare favorably with experimental observations. The role of the interfacial free-energy density and reciprocal mobility on unstable interface evolution were also examined. Sufficiently large values of the interfacial free-energy density were found to stabilize the evolution of the interface. Examinations of the deformed surface of the specimen revealed relatively large undulations, even for small perturbations from a perfect cylinder for the interface geometry.

Although our strategy makes it possible to investigate a wide range of interesting phenomena involving SRHs, a number of improvements can be envisioned. Even with enrichment, it is clear that adaptive mesh refinement would provide a more efficient means to represent the solution in the vicinity of the interface and to capture the evolving geometry of the interface. Some work along these lines using the X-FEM has been performed by Moës et al. (2003), albeit for stationary material interfaces. The use of enrichment facilitates the adaptive mesh generation because the element boundaries need not explicitly fit the interface.

Acknowledgments

John Dolbow and Huidi Ji gratefully acknowledge the support of Sandia National Laboratories through grant #184592 and NSF grant CMS-0324459. Eliot Fried gratefully acknowledges the support of NSF grant CMS-0324553. We also thank Nicolas Moës, of Ecole Centrale Nantes, for the suggestion to examine the positive-coefficient scheme and the coupling of fields between meshes.

References

Babuška, I. (1973). The finite element method with lagrangian multipliers. *Numerische Math 20*, 179–192.

Barriere, B. and L. Leibler (2003). Kinetics of solvent absorption and permeation through a highly swellable elastomeric network. *Journal of Polymer Science: Part B: Polymer Physics 41*, 166–182.

Barth, T. J. and J. Sethian (1998). Numerical schemes for the Hamilton-Jacobi and level set equations on triangulated domains. *Journal of Computational Physics 145*, 1–40.

Beebe, D. J., J. S. Moore, J. M. Bauer, Q. Yu, R. H. Liu, C. Devadoss, and B. Jo (2000). Functional hydrogel structures for autonomous flow control inside microfluidic channels. *Nature 404*, 588–590.

Belytschko, T. and T. Black (1999). Elastic crack growth in finite elements with minimal remeshing. *International Journal for Numerical Methods in Engineering 45*(5), 601–620.

Carey, G. F., S. S. Chow, and M. K. Seager (1985). Approximate boundary-flux calculations. *Computer Methods in Applied Mechanics and Engineering 50*, 107–120.

Chessa, J., P. Smolinski, and T. Belytschko (2002). Extended finite element method for solidification problems. *International Journal for Numerical Methods in Engineering 54*, 1959–1977.

Dolbow, J., N. Moës, and T. Belytschko (2000). Discontinuous enrichment in finite elements with a partition of unity method. *Finite Elements in Analysis and Design 36*, 235–260.

Dolbow, J. E., E. Fried, and H. Ji (2004). Chemically-induced swelling of hydrogels. *Journal of the Mechanics and Physics of Solids 52*, 51–84.

Duarte, C. A. and J. T. Oden (1995). hp clouds - a meshless method to solve boundary-value problems. Technical report, TICAM.

Eichenbaum, G. M., P. F. Kiser, D. Shah, S. A. Simon, and D. Needham (1999). Investigation of the swelling response and drug loading of ionic microgels: The dependence on functional group composition. *Macromolecules 32*, 8996–9006.

Fried, E. and M. E. Gurtin (1999). Coherent solid-state phase transitions with atomic diffusion: A thermomechanical treatment. *Journal of Statistical Physics 95*(5–6), 1361–1427.

Garikipati, K. and V. S. Rao (2001). Recent advances in models for thermal oxidation of silicon. *Journal of Computational Physics 174*(1), 138–170.

Gehrke, S. H., G. Agrawal, and M. C. Yang (1992). Moving ion exchange fronts in polyelectrolyte gels. *ACS Symposium Series 480*, 211–237.

Gibbs, J. W. (1878). On the equilibrium of heterogeneous substances. *Transactions of the Connecticut Academy of Arts and Sciences 3*, 108–248.

Gosz, M., J. Dolbow, and B. Moran (1998). Domain integral formulation for stress intensity factor computation along curved three-dimensional interface cracks. *International Journal of Solids and Structures 35*, 1763–1783.

Gurtin, M. E. (1995). The nature of configurational forces. *Archive for Rational Mechanics and Analysis 131*(1), 67–100.

Gurtin, M. E. (2000). *Configurational Forces as Basic Concepts in Continuum Physics*. New York: Springer.

Gurtin, M. E. and A. Struthers (1990). Evolving phase boundaries in the presence of bulk deformation. *Archive for Rational Mechanics and Analysis 112*, 97–160.

Gurtin, M. E. and P. W. Voorhees (1993). The continuum mechanics of coherent two-phase elastic solids with mass transport. *Proceedings of the Royal Society of London Series A 440*(1909), 323–343.

Ji, H., D. Chopp, and J. E. Dolbow (2002). A hybrid extended finite element/ level set method for modeling phase transformations. *International Journal for Numerical Methods in Engineering 54*, 1209–1233.

Ji, H. and J. E. Dolbow (2004). On strategies for enforcing interfacial constraints and evaluating jump conditions with the extended finite element method. *International Journal for Numerical Methods in Engineering*. Submitted for publication.

Li, F. Z., C. F. Shih, and A. Needleman (1985). A comparison of methods for calculating energy release rates. *Engineering Fracture Mechanics 21*, 405–421.

Melenk, J. M. and I. Babuška (1996). The partition of unity finite element method: Basic theory and applications. *Computer Methods in Applied Mechanics and Engineering 139*, 289–314.

Merle, R. and J. E. Dolbow (2002). Solving thermal and phase change problems with the extended finite element method. *Computational Mechanics 28*, 339–350.

Moës, N., M. Cloirec, P. Cartraud, and J. F. Remacle (2003). A computational approach to handle complex microstructure geometries. *Computer Methods in Applied Mechanics and Engineering 192*, 3163–3177.

Moës, N., J. Dolbow, and T. Belytschko (1999). A finite element method for crack growth without remeshing. *International Journal for Numerical Methods in Engineering 46*, 131–150.

Mueller, R., S. Kolling, and D. Gross (2002). On configurational forces in the context of the finite element method. *International Journal for Numerical Methods in Engineering 53*, 1557–1574.

Mullins, W. and R. Sekerka (1963). Morphological stability of a particle growing by diffusion and heat flow. *Journal of Applied Physics 34*, 323–329.

Olsen, M., J. M. Bauer, and D. Beebe (2000). Particle imaging techniques for measuring the deformation rate of hydrogel microstructures. *Applied Physics Letters 76*(22), 3310–3312.

Osher, S. and J. Sethian (1988). Fronts propagating with curvature dependent speed: Algorithms based on Hamilton-Jacobi formulation. *Journal of Computational Physics 79*, 12–49.

Pardo-Yissar, V., R. Gabai, A. N. Shipway, T. Bourenko, and I. Willner (2001). Gold nanoparticle/hydrogel composites with solvent-switchable electronic properties. *Advanced Materials 13*(17), 1320–1323.

Pehlivanov, A. I., R. D. Lazarov, and G. F. Carey (1992). Superconvergence analysis of approximate boundary-flux calculations. *Numerische Mathematik 63*, 483–501.

Rao, V. S., T. J. R. Hughes, and K. Garikipati (2000). On modeling thermal oxidation of silicon II: numerical aspects. *International Journal for Numerical Methods in Engineering 47*, 359–377.

Remacle, J. F. and C. Geuzaine (1998). Gmsh finite element grid generator. Available at www.geuz.org/gmsh.

Shih, C. F., B. Moran, and T. Nakamura (1986). Energy release rate along a three-dimensional crack front in a thermally stressed body. *International Journal of Fracture 30*, 79–102.

Steinmann, P., D. Ackermann, and F. J. Barth (2001). Application of material forces to hyperelastostatic fracture mechanics. ii. computational setting. *International Journal of Solids and Structures 38*, 5509–5526.

Sukumar, N., D. L. Chopp, N. Moës, and T. Belytschko (2001). Modeling holes and inclusions by level sets in the extended finite element method. *Computer Methods in Applied Mechanics and Engineering 190*, 6183–6200.

Tanaka, T. and D. J. Fillmore (1979). Kinetics of swelling of gels. *Journal of Chemical Physics 70*(3), 1214–1218.

Tomari, T. and M. Doi (1994). Swelling dnamics of a gel undergoing volume transitions. *Journal of the Physical Society of Japan 63*(6), 2093–2101.

Tomari, T. and M. Doi (1995). Hysteresis and incubation in the dynamics of volume transition of spherical gels. *Macromolecules 28*, 8334–8343.

List of Recent TAM Reports

No.	*Authors*	*Title*	*Date*
965	Bdzil, J. B., D. S. Stewart, and T. L. Jackson	Program burn algorithms based on detonation shock dynamics—*Journal of Computational Physics* (submitted)	Jan. 2001
966	Bagchi, P., and S. Balachandar	Linearly varying ambient flow past a sphere at finite Reynolds number: Part 2—Equation of motion—*Journal of Fluid Mechanics* **481**, 105–148 (2003) (with change in title)	Feb. 2001
967	Cermelli, P., and E. Fried	The evolution equation for a disclination in a nematic fluid—*Proceedings of the Royal Society A* **458**, 1–20 (2002)	Apr. 2001
968	Riahi, D. N.	Effects of rotation on convection in a porous layer during alloy solidification—Chapter 12 in *Transport Phenomena in Porous Media* (D. B. Ingham and I. Pop, eds.), 316–340 (2002)	Apr. 2001
969	Damljanovic, V., and R. L. Weaver	Elastic waves in cylindrical waveguides of arbitrary cross section—*Journal of Sound and Vibration* (submitted)	May 2001
970	Gioia, G., and A. M. Cuitiño	Two-phase densification of cohesive granular aggregates—*Physical Review Letters* **88**, 204302 (2002) (in extended form and with added co-authors S. Zheng and T. Uribe)	May 2001
971	Subramanian, S. J., and P. Sofronis	Calculation of a constitutive potential for isostatic powder compaction—*International Journal of Mechanical Sciences* (submitted)	June 2001
972	Sofronis, P., and I. M. Robertson	Atomistic scale experimental observations and micromechanical/continuum models for the effect of hydrogen on the mechanical behavior of metals—*Philosophical Magazine* (submitted)	June 2001
973	Pushkin, D. O., and H. Aref	Self-similarity theory of stationary coagulation—*Physics of Fluids* **14**, 694–703 (2002)	July 2001
974	Lian, L., and N. R. Sottos	Stress effects in ferroelectric thin films—*Journal of the Mechanics and Physics of Solids* (submitted)	Aug. 2001
975	Fried, E., and R. E. Todres	Prediction of disclinations in nematic elastomers—*Proceedings of the National Academy of Sciences* **98**, 14773–14777 (2001)	Aug. 2001
976	Fried, E., and V. A. Korchagin	Striping of nematic elastomers—*International Journal of Solids and Structures* **39**, 3451–3467 (2002)	Aug. 2001
977	Riahi, D. N.	On nonlinear convection in mushy layers: Part I. Oscillatory modes of convection—*Journal of Fluid Mechanics* **467**, 331–359 (2002)	Sept. 2001
978	Sofronis, P., I. M. Robertson, Y. Liang, D. F. Teter, and N. Aravas	Recent advances in the study of hydrogen embrittlement at the University of Illinois—Invited paper, Hydrogen–Corrosion Deformation Interactions (Sept. 16–21, 2001, Jackson Lake Lodge, Wyo.)	Sept. 2001
979	Fried, E., M. E. Gurtin, and K. Hutter	A void-based description of compaction and segregation in flowing granular materials—*Continuum Mechanics and Thermodynamics*, in press (2003)	Sept. 2001
980	Adrian, R. J., S. Balachandar, and Z.-C. Liu	Spanwise growth of vortex structure in wall turbulence—*Korean Society of Mechanical Engineers International Journal* **15**, 1741–1749 (2001)	Sept. 2001
981	Adrian, R. J.	Information and the study of turbulence and complex flow—*Japanese Society of Mechanical Engineers Journal B*, in press (2002)	Oct. 2001
982	Adrian, R. J., and Z.-C. Liu	Observation of vortex packets in direct numerical simulation of fully turbulent channel flow—*Journal of Visualization*, in press (2002)	Oct. 2001
983	Fried, E., and R. E. Todres	Disclinated states in nematic elastomers—*Journal of the Mechanics and Physics of Solids* **50**, 2691–2716 (2002)	Oct. 2001
984	Stewart, D. S.	Towards the miniaturization of explosive technology—Proceedings of the 23rd International Conference on Shock Waves (2001)	Oct. 2001
985	Kasimov, A. R., and Stewart, D. S.	Spinning instability of gaseous detonations—*Journal of Fluid Mechanics* (submitted)	Oct. 2001
986	Brown, E. N., N. R. Sottos, and S. R. White	Fracture testing of a self-healing polymer composite—*Experimental Mechanics* (submitted)	Nov. 2001
987	Phillips, W. R. C.	Langmuir circulations—*Surface Waves* (J. C. R. Hunt and S. Sajjadi, eds.), in press (2002)	Nov. 2001

List of Recent TAM Reports (cont'd)

No.	*Authors*	*Title*	*Date*
988	Gioia, G., and F. A. Bombardelli	Scaling and similarity in rough channel flows—*Physical Review Letters* **88**, 014501 (2002)	Nov. 2001
989	Riahi, D. N.	On stationary and oscillatory modes of flow instabilities in a rotating porous layer during alloy solidification—*Journal of Porous Media* **6**, 1–11 (2003)	Nov. 2001
990	Okhuysen, B. S., and D. N. Riahi	Effect of Coriolis force on instabilities of liquid and mushy regions during alloy solidification—*Physics of Fluids* (submitted)	Dec. 2001
991	Christensen, K. T., and R. J. Adrian	Measurement of instantaneous Eulerian acceleration fields by particle-image accelerometry: Method and accuracy—*Experimental Fluids* (submitted)	Dec. 2001
992	Liu, M., and K. J. Hsia	Interfacial cracks between piezoelectric and elastic materials under in-plane electric loading—*Journal of the Mechanics and Physics of Solids* **51**, 921–944 (2003)	Dec. 2001
993	Panat, R. P., S. Zhang, and K. J. Hsia	Bond coat surface rumpling in thermal barrier coatings—*Acta Materialia* **51**, 239–249 (2003)	Jan. 2002
994	Aref, H.	A transformation of the point vortex equations—*Physics of Fluids* **14**, 2395–2401 (2002)	Jan. 2002
995	Saif, M. T. A, S. Zhang, A. Haque, and K. J. Hsia	Effect of native Al_2O_3 on the elastic response of nanoscale aluminum films—*Acta Materialia* **50**, 2779–2786 (2002)	Jan. 2002
996	Fried, E., and M. E. Gurtin	A nonequilibrium theory of epitaxial growth that accounts for surface stress and surface diffusion—*Journal of the Mechanics and Physics of Solids* **51**, 487–517 (2003)	Jan. 2002
997	Aref, H.	The development of chaotic advection—*Physics of Fluids* **14**, 1315–1325 (2002); see also *Virtual Journal of Nanoscale Science and Technology*, 11 March 2002	Jan. 2002
998	Christensen, K. T., and R. J. Adrian	The velocity and acceleration signatures of small-scale vortices in turbulent channel flow—*Journal of Turbulence*, in press (2002)	Jan. 2002
999	Riahi, D. N.	Flow instabilities in a horizontal dendrite layer rotating about an inclined axis—*Journal of Porous Media*, in press (2003)	Feb. 2002
1000	Kessler, M. R., and S. R. White	Cure kinetics of ring-opening metathesis polymerization of dicyclopentadiene—*Journal of Polymer Science A* **40**, 2373–2383 (2002)	Feb. 2002
1001	Dolbow, J. E., E. Fried, and A. Q. Shen	Point defects in nematic gels: The case for hedgehogs—*Proceedings of the National Academy of Sciences* (submitted)	Feb. 2002
1002	Riahi, D. N.	Nonlinear steady convection in rotating mushy layers—*Journal of Fluid Mechanics* **485**, 279–306 (2003)	Mar. 2002
1003	Carlson, D. E., E. Fried, and S. Sellers	The totality of soft-states in a neo-classical nematic elastomer—*Journal of Elasticity* **69**, 169–180 (2003) with revised title	Mar. 2002
1004	Fried, E., and R. E. Todres	Normal-stress differences and the detection of disclinations in nematic elastomers—*Journal of Polymer Science B: Polymer Physics* **40**, 2098–2106 (2002)	June 2002
1005	Fried, E., and B. C. Roy	Gravity-induced segregation of cohesionless granular mixtures—*Lecture Notes in Mechanics*, in press (2002)	July 2002
1006	Tomkins, C. D., and R. J. Adrian	Spanwise structure and scale growth in turbulent boundary layers—*Journal of Fluid Mechanics* (submitted)	Aug. 2002
1007	Riahi, D. N.	On nonlinear convection in mushy layers: Part 2. Mixed oscillatory and stationary modes of convection—*Journal of Fluid Mechanics* (submitted)	Sept. 2002
1008	Aref, H., P. K. Newton, M. A. Stremler, T. Tokieda, and D. L. Vainchtein	Vortex crystals—*Advances in Applied Mathematics* **39**, in press (2002)	Oct. 2002
1009	Bagchi, P., and S. Balachandar	Effect of turbulence on the drag and lift of a particle—*Physics of Fluids*, in press (2003)	Oct. 2002

List of Recent TAM Reports (cont'd)

No.	*Authors*	*Title*	*Date*
1010	Zhang, S., R. Panat, and K. J. Hsia	Influence of surface morphology on the adhesive strength of aluminum/epoxy interfaces—*Journal of Adhesion Science and Technology* **17**, 1685–1711 (2003)	Oct. 2002
1011	Carlson, D. E., E. Fried, and D. A. Tortorelli	On internal constraints in continuum mechanics—*Journal of Elasticity* **70**, 101–109 (2003)	Oct. 2002
1012	Boyland, P. L., M. A. Stremler, and H. Aref	Topological fluid mechanics of point vortex motions—*Physica D* **175**, 69–95 (2002)	Oct. 2002
1013	Bhattacharjee, P., and D. N. Riahi	Computational studies of the effect of rotation on convection during protein crystallization—*International Journal of Mathematical Sciences*, in press (2004)	Feb. 2003
1014	Brown, E. N., M. R. Kessler, N. R. Sottos, and S. R. White	*In situ* poly(urea-formaldehyde) microencapsulation of dicyclopentadiene—*Journal of Microencapsulation* (submitted)	Feb. 2003
1015	Brown, E. N., S. R. White, and N. R. Sottos	Microcapsule induced toughening in a self-healing polymer composite—*Journal of Materials Science* (submitted)	Feb. 2003
1016	Kuznetsov, I. R., and D. S. Stewart	Burning rate of energetic materials with thermal expansion—*Combustion and Flame* (submitted)	Mar. 2003
1017	Dolbow, J., E. Fried, and H. Ji	Chemically induced swelling of hydrogels—*Journal of the Mechanics and Physics of Solids*, in press (2003)	Mar. 2003
1018	Costello, G. A.	Mechanics of wire rope—Mordica Lecture, Interwire 2003, Wire Association International, Atlanta, Georgia, May 12, 2003	Mar. 2003
1019	Wang, J., N. R. Sottos, and R. L. Weaver	Thin film adhesion measurement by laser induced stress waves—*Journal of the Mechanics and Physics of Solids* (submitted)	Apr. 2003
1020	Bhattacharjee, P., and D. N. Riahi	Effect of rotation on surface tension driven flow during protein crystallization—*Microgravity Science and Technology* **14**, 36–44 (2003)	Apr. 2003
1021	Fried, E.	The configurational and standard force balances are not always statements of a single law—*Proceedings of the Royal Society* (submitted)	Apr. 2003
1022	Panat, R. P., and K. J. Hsia	Experimental investigation of the bond coat rumpling instability under isothermal and cyclic thermal histories in thermal barrier systems—*Proceedings of the Royal Society of London A*, in press (2003)	May 2003
1023	Fried, E., and M. E. Gurtin	A unified treatment of evolving interfaces accounting for small deformations and atomic transport: grain-boundaries, phase transitions, epitaxy—*Advances in Applied Mechanics*, in press (2003)	May 2003
1024	Dong, F., D. N. Riahi, and A. T. Hsui	On similarity waves in compacting media—*Horizons in Physics*, in press (2003)	May 2003
1025	Liu, M., and K. J. Hsia	Locking of electric field induced non-180° domain switching and phase transition in ferroelectric materials upon cyclic electric fatigue—*Applied Physics Letters*, in press (2003)	May 2003
1026	Liu, M., K. J. Hsia, and M. Sardela Jr.	In situ X-ray diffraction study of electric field induced domain switching and phase transition in PZT-5H—*Journal of the American Ceramics Society* (submitted)	May 2003
1027	Riahi, D. N.	On flow of binary alloys during crystal growth—*Recent Research Development in Crystal Growth*, in press (2003)	May 2003
1028	Riahi, D. N.	On fluid dynamics during crystallization—*Recent Research Development in Fluid Dynamics*, in press (2003)	July 2003
1029	Fried, E., V. Korchagin, and R. E. Todres	Biaxial disclinated states in nematic elastomers—*Journal of Chemical Physics* **119**, 13170–13179 (2003)	July 2003
1030	Sharp, K. V., and R. J. Adrian	Transition from laminar to turbulent flow in liquid filled microtubes—*Physics of Fluids* (submitted)	July 2003

List of Recent TAM Reports (cont'd)

No.	*Authors*	*Title*	*Date*
1031	Yoon, H. S., D. F. Hill, S. Balachandar, R. J. Adrian, and M. Y. Ha	Reynolds number scaling of flow in a Rushton turbine stirred tank: Part I—Mean flow, circular jet and tip vortex scaling—*Chemical Engineering Science* (submitted)	Aug. 2003
1032	Raju, R., S. Balachandar, D. F. Hill, and R. J. Adrian	Reynolds number scaling of flow in a Rushton turbine stirred tank: Part II—Eigen-decomposition of fluctuation—*Chemical Engineering Science* (submitted)	Aug. 2003
1033	Hill, K. M., G. Gioia, and V. V. Tota	Structure and kinematics in dense free-surface granular flow—*Physical Review Letters*, in press (2003)	Aug. 2003
1034	Fried, E., and S. Sellers	Free-energy density functions for nematic elastomers—*Journal of the Mechanics and Physics of Solids* **52**, 1671–1689 (2004)	Sept. 2003
1035	Kasimov, A. R., and D. S. Stewart	On the dynamics of self-sustained one-dimensional detonations: A numerical study in the shock-attached frame—*Physics of Fluids* (submitted)	Nov. 2003
1036	Fried, E., and B. C. Roy	Disclinations in a homogeneously deformed nematic elastomer—*Nature Materials* (submitted)	Nov. 2003
1037	Fried, E., and M. E. Gurtin	The unifying nature of the configurational force balance—*Mechanics of Material Forces* (P. Steinmann and G. A. Maugin, eds.), in press (2003)	Dec. 2003
1038	Panat, R., K. J. Hsia, and J. W. Oldham	Rumpling instability in thermal barrier systems under isothermal conditions in vacuum—*Philosophical Magazine* (submitted)	Dec. 2003
1039	Cermelli, P., E. Fried, and M. E. Gurtin	Sharp-interface nematic–isotropic phase transitions without flow—*Archive for Rational Mechanics and Analysis* (submitted)	Dec. 2003
1040	Yoo, S., and D. S. Stewart	A hybrid level-set method in two and three dimensions for modeling detonation and combustion problems in complex geometries—*Combustion Theory and Modeling* (submitted)	Feb. 2004
1041	Dienberg, C. E., S. E. Ott-Monsivais, J. L. Ranchero, A. A. Rzeszutko, and C. L. Winter	Proceedings of the Fifth Annual Research Conference in Mechanics (April 2003), TAM Department, UIUC (E. N. Brown, ed.)	Feb. 2004
1042	Kasimov, A. R., and D. S. Stewart	Asymptotic theory of ignition and failure of self-sustained detonations—*Journal of Fluid Mechanics* (submitted)	Feb. 2004
1043	Kasimov, A. R., and D. S. Stewart	Theory of direct initiation of gaseous detonations and comparison with experiment—*Proceedings of the Combustion Institute* (submitted)	Mar. 2004
1044	Panat, R., K. J. Hsia, and D. G. Cahill	Evolution of surface waviness in thin films via volume and surface diffusion—*Journal of Applied Physics* (submitted)	Mar. 2004
1045	Riahi, D. N.	Steady and oscillatory flow in a mushy layer—*Current Topics in Crystal Growth Research* (submitted)	Mar. 2004
1046	Riahi, D. N.	Modeling flows in protein crystal growth—*Current Topics in Crystal Growth Research* (submitted)	Mar. 2004
1047	Bagchi, P., and S. Balachandar	Response of the wake of an isolated particle to isotropic turbulent cross-flow—*Journal of Fluid Mechanics* (submitted)	Mar. 2004
1048	Brown, E. N., S. R. White, and N. R. Sottos	Fatigue crack propagation in microcapsule toughened epoxy—*Journal of Materials Science* (submitted)	Apr. 2004
1049	Zeng, L., S. Balachandar, and P. Fischer	Wall-induced forces on a rigid sphere at finite Reynolds number—*Journal of Fluid Mechanics* (submitted)	May 2004
1050	Dolbow, J., E. Fried, and H. Ji	A numerical strategy for investigating the kinetic response of stimulus-responsive hydrogels—*Journal of the Mechanics and Physics of Solids* (submitted)	June 2004